ORNL/TM-2019/1400

SCALE Lattice Physics Code Assessments of Accident-Tolerant Fuel

Matthew Jessee
Jinan Yang
Ugur Mertyurek
William Marshall
Andrew Holcomb

June 18, 2020

OAK RIDGE NATIONAL LABORATORY
MANAGED BY UT-BATTELLE FOR THE US DEPARTMENT OF ENERGY

ORNL/TM-2019/1400

Reactor and Nuclear Systems Division

SCALE LATTICE PHYSICS CODE ASSESSMENTS OF ACCIDENT-TOLERANT FUEL

Matthew Jessee
Jinan Yang
Ugur Mertyurek
William Marshall
Andrew Holcomb

Date Published: June 18, 2020

Prepared by
OAK RIDGE NATIONAL LABORATORY
Oak Ridge, TN 37831-6283
managed by
UT-Battelle, LLC
for the
US DEPARTMENT OF ENERGY
under contract DE-AC05-00OR22725

CONTENTS

LIST OF FIGURES

LIST OF TABLES

ACRONYMS

β	effective delayed neutron fraction
ϵ	fast fission factor
η*f	(reproduction factor * thermal utilization factor)
λ	precursor decay constant
ϕ_1/ϕ_2	fast to thermal flux ratio
AOO	anticipated operational occurence
ATF	accident-tolerant fuel
BOC	beginning of cycle
BOL	beginning of life
BWR	boiling water reactor
CE	continuous energy
CRW	control rod worth
DBA	design basis accident
DBW	differential boron worth
DOM	dominant zone
DTC	Doppler temperature coefficient
EOC	end of cycle
EOL	end of life
FG	few group
HFP	hot full power
LEU	low enriched uranium
LTA	lead test assembly
LTR	lead test rod
LWR	light water reactor
MC	Monte Carlo
MG	multigroup
MIX	mixture of uranium and plutonium
MOC	method of characteristics
MTC	moderator temperature coefficient
NRC	US Nuclear Regulatory Commission
ORNL	Oak Ridge National Laboratory
p	resonance escape probability
pcm	per cent mille
PWR	pressurized water reactor
QOI	quantity of interest
RSD	relative standard deviation
S/U	sensitivity and uncertainty
UM	University of Michigan

ACKNOWLEDGMENTS

The authors would like to thank Don Algama (US Nuclear Regulatory Commission (NRC)) and Brad Rearden (Oak Ridge National Laboratory (ORNL)) for their guidance and oversight for this project. The authors would also like to thank the following staff for their input into the scope of work: Ian Porter (formerly NRC), Andrew Bielen (NRC), Nathanael Hudson (NRC), William Wieselquist (ORNL), Jeffrey Powers (ORNL), Kurt Terrani (ORNL), and Andrew Ward (University of Michigan (UM)). We express special thanks and acknowledgment of the contribution of Stephen (Steve) Bowman (ORNL) to this work. Steve was the original ORNL project manager before retiring in February 2018 and passing away in October 2018. His leadership and project management were essential in initiating the work documented in this report.

ABSTRACT

This report highlights accident-tolerant fuel (ATF) code assessment activities performed under Project NRC-HQ-60-17-T-0017, Lattice Physics Enhancements and Assessment. ATF covers a broad range of advanced fuel and clad designs for light water reactors (LWRs) to enhance performance under several accident conditions. Several ATF concepts are anticipated to be deployed as lead test rods (LTRs) or lead test assemblies (LTAs) within the next five years. The purpose of this work is to assess the predictive capabilities of NRC neutronics codes that underpin various licensing calculations.

ATF designs use different fuel and clad materials compared to standard UO_2 fuel and zirconium-alloy claddings (hereafter UO_2-Zry). These new materials and geometrical designs need to be assessed to quantify the impact of nuclear data uncertainties on quantities of interest (QOIs) in licensing calculations and the impact of modeling approximations which may be valid for UO_2-Zry but not for ATF. This report outlines a systematic approach for ATF neutronics code assessment which includes sensitivity and uncertainty (S/U) analysis of nuclear data, identification of experimental benchmark and gaps for code validation, investigation of modeling approximations, and code-to-code comparisons of calculated QOIs against high-fidelity reference continuous energy (CE) Monte Carlo (MC) calculations.

This report focuses on the assessment of the SCALE/Polaris lattice physics code for reactor safety analysis. Polaris lattice physics calculations generate few group (FG) cross sections for PARCS full-core calculations. (Full-core analysis, spent fuel analysis, and severe accident analysis will be performed in future work.) The selected ATF concepts for this report include Cr_2O_3 and Al_2O_3-Cr_2O_3-doped UO_2 fuel, U_3Si_2 fuel, FeCrAl cladding, SiC cladding, and Cr-coated cladding.

1. INTRODUCTION

ATF covers a broad range of advanced fuel and clad designs for LWRs to enhance performance under several accident conditions and normal operation. As several ATF concepts are to be deployed as LTRs or LTAs within the next five years, NRC codes (SCALE, PARCS, TRACE, FAST, MELCOR, MACCS2) must be assessed to understand if existing models and data are valid for ATF licensing calculations. The primary focus of this report is on the assessment of SCALE/Polaris (Jessee et al. 2014) for generating FG cross sections for PARCS for ATF reactor safety calculations. PARCS core calculations can be either stand-alone, steady-state core depletion calculations, or they can be coupled to TRACE for analysis of anticipated operational occurences (AOOs) or design basis accidents (DBAs). Additionally, Polaris is also used to characterize fuel isotopics as a function of burnup, which are used as input parameters for MELCOR and MACCS2 severe accident calculations and spent fuel storage and transportation calculations.

ATF designs use different fuel and clad materials compared to standard UO_2-Zry. These new materials and geometrical designs must be assessed to quantify the impact of nuclear data uncertainties on QOIs and the impact of modeling approximations which may be valid for UO_2-Zry but not for ATF. ATF concepts for this report include Cr_2O_3 and Al_2O_3-Cr_2O_3-doped UO_2 fuel, U_3Si_2 fuel, FeCrAl cladding, SiC cladding, and Cr-coated cladding. Specific designs evaluated in this work are provided in Table 2.

Table 2. Selected ATF lattice designs

Reactor type	Fuel	Clad
PWR WEC 17×17 (Baseline)	UO_2	Zircaloy-4
PWR WEC 17×17	Al_2O_3-Cr_2O_3 doped UO_2	Cr-coated Zircaloy-4
PWR WEC 17×17	Cr_2O_3 doped UO_2	Cr-coated M5
PWR WEC 17×17	Cr_2O_3 doped UO_2	SiC
PWR WEC 17×17	U_3Si_2	SiC
PWR WEC 17×17	U_3Si_2	Cr-coated Zircaloy-4
BWR GE14 10×10 (Baseline)[a]	UO_2	Zircaloy-2
BWR GE14 10×10	UO_2	Cr-coated Zircaloy-2
BWR GE14 10×10	UO_2	FeCrAl
BWR GE14 10×10	UO_2 (optimized)[b]	FeCrAl
BWR ATRIUM 11×11 (Baseline)[c]	UO_2	Zircaloy-2
BWR ATRIUM 11×11	Cr_2O_3 doped UO_2	Zircaloy-2

[a] ^{235}U and Gd_2O_3 distributions from (Fensin 2004).
[b] See Section 3.2 for details.
[c] Generic 11×11 ATRIUM design.

This report is organized as follows. Section 2 focuses on the impact of nuclear data uncertainties on ATF neutronics calculations and the identification of available experimental benchmarks for code validation. Section 3 investigates different modeling approximations for ATF calculations with Polaris. Section 4 summarizes code-to-code comparisons of QOIs between Polaris and reference CE MC solutions for lattice physics calculations for a wide range of normal and accident conditions. Section 5 summarizes the code enhancements introduced into Polaris as part of this project. Conclusions of the report and recommendations for future work are provided in Section 6. Calculation notebooks are provided in the appendix of the report, which summarizes the model descriptions for the code assessment analysis in Section 4.

Both SCALE 6.3 and SCALE 6.2.3 (Rearden and M. A. Jessee, Eds. 2016) were used for calculations in this report. The SCALE 6.2.3 code system includes Polaris for lattice physics, CE KENO for reference solutions, TSUNAMI-3D for S/U analysis, TSUNAMI-IP for benchmark similarity analysis, and Sampler for depletion uncertainty analysis. SCALE 6.3 was used to provide Shift-based reference MC solutions for Polaris assessments in Section 4.

2. BENCHMARK IDENTIFICATION

ATF introduces new fuel and cladding materials to LWR assembly designs. Some of these materials have never been used in reactors or critical experiments, and others have not been used in significant quantities. This section outlines the sensitivity, uncertainty, and similarity assessment calculations performed to determine what experimental data are available for neutronics code validation for ATF.

TSUNAMI-3D was used to generate the sensitivity data for each lattice in Table 2, and the SCALE 56-group covariance library was used for all uncertainty and similarity calculations. These results were presented to the criticality safety community at two conferences in 2019 (Marshall, Yang, et al. 2019; Marshall, Clarity, et al. 2019).

2.1 SENSITIVITY AND UNCERTAINTY ANALYSIS

The nuclear data induced uncertainty in k_{eff} can be calculated by SCALE TSUNAMI-3D sequences by propagating the covariance data with the application-specific sensitivities. The uncertainty is determined for each of several reactions for each isotope, and these reaction- and isotope-specific uncertainties are combined to determine the total uncertainty in k_{eff} due to the uncertainties in the nuclear data used in the model. Table 3 provides the total data-induced uncertainties for the pressurized water reactor (PWR) ATF concepts. The uncertainty is presented as the relative standard deviation (RSD) in k_{eff} in per cent mille (pcm). The UO_2-Zry and ATF lattices have similar total uncertainties, with a small increase for the U_3Si_2 lattices.

Table 3. Total data-induced uncertainty in k_{eff} in PWR ATF designs

Fuel	Clad	Data-induced uncertainty (pcm)
UO_2 (Baseline)	Zircaloy-4	544
Al_2O_3-Cr_2O_3 doped UO_2	Cr-coated Zircaloy-4	551
Cr_2O_3 doped UO_2	Cr-coated M5	548
Cr_2O_3 doped UO_2	SiC	545
U_3Si_2	SiC	571
U_3Si_2	Cr-coated Zircaloy-4	571

The top ten isotopes contributing to uncertainty are provided in Table 4. [1] In all six cases, these ten individual reactions contribute at least 99.98% of the total uncertainty shown in Table 3. The top three contributors in all cases are ranked as (1) ^{235}U, (2) ^{238}U, and (3) ^{1}H. It is a significant conclusion that the top three contributors do not change with doping elements, the U_3Si_2 fuel, or any of the cladding concepts. The total uncertainty in U_3Si_2-fueled systems is slightly higher than UO_2fueled systems. The U_3Si_2-fueled concepts have a harder neutron spectrum, resulting in the higher sensitivity to ^{238}U inelastic scattering.

The total data-induced uncertainties for the boiling water reactor (BWR) systems are presented for each concept in Table 5. The introduction of chromium doping has essentially no impact on total uncertainty, which is similar to the impact for the PWR systems. The introduction of FeCrAl cladding increases the total uncertainty by about 50 pcm, but this effect is lessened with an optimization of the enrichments and dimensions of the lattice to offset the reactivity impacts of the new cladding material.

1. The uncertainty contributed by each reaction has been summed to simplify presentation.

Table 4. Top ten isotopes contributing to data-induced uncertainty in PWR ATF designs

UO_2 Zirc-4		Al_2O_3-Cr_2O_3 dopant Cr coated Zirc-4		Cr_2O_3 dopant Cr coated M5		Cr_2O_3 dopant SiC clad		U_3Si_2 fuel SiC clad		U_3Si_2 fuel Cr coated Zirc-4	
Nuclide	Unc.	Nuclide	Unc.	Nuclide	Unc.	Nuclide	Unc.	Nuclide	Unc.	Nuclide	Unc.
^{235}U	445	^{235}U	450	^{235}U	447	^{235}U	444	^{235}U	453	^{235}U	458
^{238}U	307	^{238}U	312	^{238}U	312	^{238}U	312	^{238}U	343	^{238}U	336
^{1}H	46	^{1}H	46	^{1}H	46	^{1}H	46	^{1}H	41	^{1}H	41
^{91}Zr	26	^{91}Zr	25	^{91}Zr	25	^{16}O	22	^{28}Si	31	^{91}Zr	23
^{92}Zr	21	^{16}O	21	^{16}O	22	^{28}Si	13	^{30}Si	10	^{28}Si	18
^{16}O	21	^{92}Zr	20	^{92}Zr	21	^{10}B	9	^{234}U	8	^{92}Zr	18
^{90}Zr	10	^{90}Zr	10	^{90}Zr	10	^{234}U	7	^{10}B	8	^{90}Zr	10
^{10}B	9	^{10}B	9	^{10}B	9	^{30}Si	4	^{16}O	5	^{234}U	8
^{234}U	7	^{53}Cr	8	^{234}U	7	^{91}Zr	2	^{236}U	2	^{10}B	8
^{94}Zr	4	^{234}U	7	^{93}Nb	6	^{92}Zr	2	^{91}Zr	2	^{53}Cr	7

Table 5. Total data-induced uncertainty in k_{eff} in BWR ATF designs

Fuel	Clad	Data-induced uncertainty (pcm)
GE14 10×10 UO_2 (Baseline)	Zircaloy-2	614
GE14 10×10 UO_2	Cr-coated Zircaloy-2	616
GE14 10×10 UO_2	FeCrAl	661
GE14 10×10 UO_2 (optimized)	FeCrAl	632

The top ten isotopes contributing to uncertainty are presented in Table 6. In all cases, the top ten isotopes contribute at least 99.8% of the total uncertainty. The addition of FeCrAl cladding introduces ^{56}Fe as a large contributor which is responsible for the increase in total uncertainty. The optimization reduces the ^{56}Fe sensitivity, and thus reduces its contribution to uncertainty, returning ^{157}Gd to the third most important contributor. In the optimized FeCrAl case, the contributions from Gd isotopes is actually lower than in the UO_2-Zry cases. The ^{56}Fe contribution is also reduced compared to the direct implementation of FeCrAl, but the total uncertainty remains higher than in the UO_2-Zry cases. The Gd isotopes contributing to total uncertainty are residual burnable absorbers, and the Zr contributions in the FeCrAl case come from the use of Zircaloy in the GE14 assembly's water tubes.

The total data-induced uncertainty in both the PWR and BWR systems shows mild increases caused by the introduction of ATF concepts. The uncertainty in the PWR systems increases by no more than 30 pcm, which is only about a 5% increase. The primary change that increases uncertainty at all is the introduction of U_3Si_2 fuel and the associated mild spectral hardening. For the BWR systems, the largest increase was almost 50 pcm, or 8%, and was caused by the introduction of FeCrAl cladding. Optimization of the FeCrAl lattice to offset the reactivity impact of Cr absorption lessened the uncertainty increase. Though not examined here, the introduction of FeCrAl cladding into a PWR system should be on the same order as that seen for BWR systems. The impact may be slightly higher, as the PWR systems have a slightly softer spectrum than the BWR dominant zone (DOM) lattice considered here. Similarly, the use of U_3Si_2 fuel in a BWR would likely result in a similar impact on the total uncertainty, as seen for the PWR systems. The harder spectrum in the BWR models might serve to lower the impact. Based on these calculations, the introduction of these ATF concepts does not significantly increase the data-induced uncertainty in commercial LWR systems.

Table 6. Top ten isotopes contributing to data-induced uncertainty in BWR ATF designs

GE14 10×10							
UO_2 Zirc-2		UO_2 Cr coated Zirc-2		UO_2 FeCrAl		UO_2 (opt.) FeCrAl	
Nuclide	Unc.	Nuclide	Unc.	Nuclide	Unc.	Nuclide	Unc.
^{235}U	473	^{235}U	476	^{235}U	478	^{235}U	476
^{238}U	310	^{238}U	310	^{238}U	314	^{238}U	341
^{157}Gd	196	^{157}Gd	194	^{56}Fe	247	^{157}Gd	173
^{155}Gd	101	^{155}Gd	100	^{157}Gd	181	^{56}Fe	112
^{1}H	56	^{1}H	56	^{155}Gd	95	^{155}Gd	97
^{91}Zr	49	^{91}Zr	49	^{1}H	54	^{1}H	49
^{92}Zr	44	^{92}Zr	43	^{91}Zr	28	^{91}Zr	26
^{90}Zr	21	^{90}Zr	20	^{92}Zr	26	^{92}Zr	23
^{156}Gd	19	^{16}O	20	^{53}Cr	23	^{16}O	23
^{16}O	19	^{156}Gd	19	^{16}O	20	^{156}Gd	20

2.2 SIMILARITY ANALYSIS TO BENCHMARK EXPERIMENTS

Each of the ATF lattices was compared against a suite of critical experiments to identify potential experiments for code validation. A suite of 1,643 critical experiments fueled with low enriched uranium (LEU), or a mixture of uranium and plutonium (MIX) was assembled for previous work examining the validation of BWR fuel assemblies (Marshall et al. 2015). The fissile material in the experiments is generally oxide fuel rods arranged in an array in light water, but some LEU and MIX solutions are also considered as potential critical experiments for validation.

The ATF lattices used to generate sensitivity data were modeled at beginning of life (BOL) hot full power (HFP) conditions. A total of 48 critical experiments were identified with a similarity factor (c_k) of 0.8 or more. These experiments were all drawn from LEU-COMP-THERM (LCT) evaluations, including cases from LCT-005, LCT-008, LCT-011, LCT-014, LCT-051, and LCT-076. The highest c_k value for any experiment was 0.959. The c_k values for most experiments would increase if the ATF lattice models were modelled at room temperature, as nearly all of the experiments were performed at ambient conditions, but analysis of the KRITZ benchmark suggests that the temperature effect would increase c_k by 0.05.

The primary concern in this study is how the introduction of ATF fuel concepts might change the set of applicable experiments that would be used to perform validation. The UO_2-fueled ATF concepts suffer only small reductions in the number of potentially applicable experiments identified and the maximum c_k value, as shown in Table 7. Modest reductions in the number of applicable experiments are evident for the Cr_2O_3- and Al_2O_3-Cr_2O_3-doped $UO_2$with Zircaloy, the M5 cladding with Cr_2O_3-doped UO_2, and the Cr_2O_3-doped UO_2 with SiC clad. The maximum c_k values for the base case and these three ATF concepts are between 0.95 and 0.96. Both U_3Si_2-fueled ATF concepts have fewer identified applicable experiments and noticeably lower maximum c_k values of approximately 0.93. As with the data-induced uncertainties discussed in the

previous section, the introduction of ATF concepts does not significantly reduce the applicability of critical experiments for validation. The U_3Si_2-fueled concepts do show fewer applicable experiments from the suite of critical experiments used, but no attempt was made to find experiments fueled with U_3Si_2. This is a fuel material used in some research reactors (Author unspecified 2006), so benchmarks may exist, or operating data could be used for validation for these reactors.

Table 7. Summary of applicable experiments to PWR ATF designs

Fuel	Clad	Number of experiments with $c_k \geq 0.8$	Maximum c_k value
UO_2 (Baseline)	Zircaloy-4	48	0.959
Al_2O_3-Cr_2O_3 doped UO_2	Cr-coated Zircaloy-4	40	0.952
Cr_2O_3 doped UO_2	Cr-coated M5	42	0.954
Cr_2O_3 doped UO_2	SiC	43	0.956
U_3Si_2	SiC	25	0.929
U_3Si_2	Cr-coated Zircaloy-4	25	0.932

As with the PWR lattices, each of the BWR lattices was compared against the suite of 1,643 experiments to determine potentially applicable experiments. The suite of available critical benchmarks generally shows lower applicability to BWR fuel than to PWR fuel (Scaglione et al. 2012), so fewer experiments were expected to be applicable. As expected, the base UO_2-Zry case has fewer potentially applicable experiments (14) than the PWR case (48). The maximum c_k is approximately 0.83, and all 14 cases come from LCT-008. The applicability of this particular evaluation to BWR fuel has been shown in other studies as well (Marshall et al. 2015). Also, as with the PWR systems, it is expected that c_k values would increase for most critical experiments if compared to a reactor model at room temperature.

The applicability of critical experiments from the suite for the Cr-coated Zircaloy is similar to the base case but FeCrAl concepts present validation challenges, as shown in 8. The Cr-coated Zircaloy lattice changes neither the number of applicable experiments nor the maximum c_k value. The unoptimized and optimized FeCrAl models have 1 and 2 experiments with c_k values of at least 0.8, respectively, and maximum c_k values of approximately 0.80. The single applicable case for the unoptimized FeCrAl lattice is LCT-076 Case 4; the LCT-076 experiments are likely more applicable because of the harder neutron energy spectrum and the use of stainless steel clad fuel rods. Like the base case, the other ATF concepts draw their high c_k experiments from the LCT-008 evaluation. In summary, validation of BWR lattices is more difficult with the existing suite of critical experiments, and the introduction of FeCrAl cladding exacerbates these difficulties.

Table 8. Summary of applicable experiments to BWR ATF designs

Fuel	Clad	Number of experiments with $c_k \geq 0.8$	Maximum c_k value
GE14 10×10 UO_2 (Baseline)	Zircaloy-2	14	0.828
GE14 10×10 UO_2	Cr-coated Zircaloy-2	14	0.828
GE14 10×10 UO_2	FeCrAl	1	0.801
GE14 10×10 UO_2 (optimized)	FeCrAl	2	0.803

3. POLARIS MODELING INVESTIGATIONS

This section highlights several parametric studies performed to understand modeling limitations for ATF, such as the modeling of small clad coatings, the reactivity effect of FeCrAl cladding, Cr_2O_3 dopants and Cr-coats, and the use of U_3Si_2 fuel compared to the conventional UO_2 fuel.

3.1 CHROMIUM COAT MODEL

Compared to traditional UO_2-Zry fuel, thin ceramic coating at the exterior of the cladding can be used to potentially limit oxidation and hydrogen pick-up during normal operating conditions or to limit hydrogen production during accident scenarios. Depending on the cladding materials, the ceramic coatings vary from 10–30 μm in thickness. Explicit modeling of these ceramic coatings is difficult in Polaris, requiring fine ray-spacing selection for the method of characteristics (MOC) transport solver, which increases run time. To reduce the Polaris run time, six different coat homogenization options were considered and compared against an explicit model. This study was performed for a WEC 17×17 lattice with 30 μm Cr coat. The Zircaloy-4 clad thickness for this design is 570 μm. The six different coat homogenization options are as follows:

1. The 30 μm coat is homogenized with 570 μm of clad. The homogenized clad thickness is 600 μm.
2. The 30 μm coat is homogenized with the 570 μm of clad. The homogenized clad thickness is set to 570 μm, with the homogenized clad density adjusted to preserve the mass of Zircaloy and Cr coat. (This case preserves the nominal clad thickness.)
3. The 30 μm coat is homogenized with the 540 μm of clad. The total clad thickness is 570 μm. (This case removes 30 μm of Zircaloy to preserve the nominal clad thickness.)
4. The 30 μm coat is homogenized with the outer 30 μm of clad. The homogenized clad thickness is 600 μm (540 μm of Ziraloy and 60 μm of homogenized Zircaloy and Cr).
5. The 30 μm coat is homogenized with the outer 60 μm of clad. The homogenized clad thickness is 600 μm (510 μm of Zircolay and 90 μm of homogenized Zircaloy and Cr).
6. The 30 μm coat is homogenized with the outer 270 μm of clad. The homogenized clad thickness is 600 μm (300 μm of Zircaloy and 300 μm of homogenized Zircaloy and Cr).

These six options are labeled in the figures that follow as *coating homog-1* through *coating homog-6*. For each case, 13 different Polaris calculations were performed using the BOL state conditions provided in Table 9. Using Polaris calculations with explicit Cr coating as the basis for comparing the homogenization options, k_{inf} differences are presented in Figure 1(a) through Figure 1(f). Clearly, options coating homog-1, -4, -5, and -6 have little impact on the k_{inf} values. coating homog-2 and -3 changed k_{inf} up to 210 pcm. The main effect in these two cases is that the original clad thickness (570 μm) is preserved, which implies that the moderator volume is larger than that in the reference Polaris calculation. From these calculations, the approach used in coating homog-6 is recommended for homogenizing the coat with the cladding. The reactivity difference is small, and it essentially splits the clad model into two 300 μm thick regions, which does not impact the ray spacing selection in Polaris and it accurately models the parasitic absorption of the Cr coat. This homogenization option is used for the Polaris-to–CE Shift assessment in Section 4.

Table 9. PWR BOL cases for Cr coat homogenization study

Case number	Fuel temp (K)	System temp (K)	Boron conc (ppm)
1	293	293	0
2	293	293	1,000
3	293	293	1,300
4	293	293	2,000
5	293	293	2,500
6	560	560	0
7	560	560	1000
8	560	560	1,300
9	560	560	2,000
10	560	560	2,500
11	900	560	1,300
12	900	600	1,300
13	1,800	560	1,300

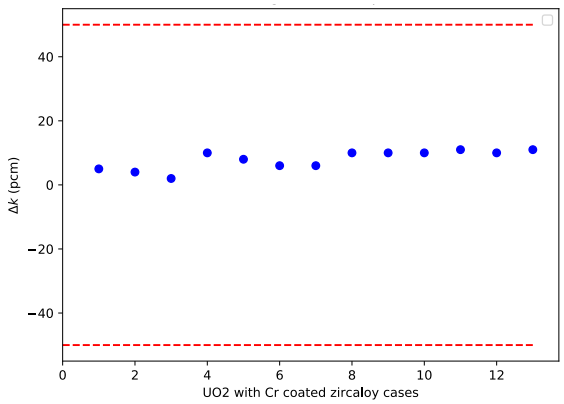

(a) Coating homog-1

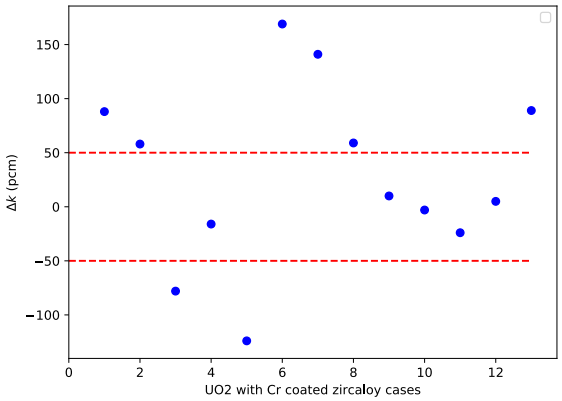

(b) Coating homog-2

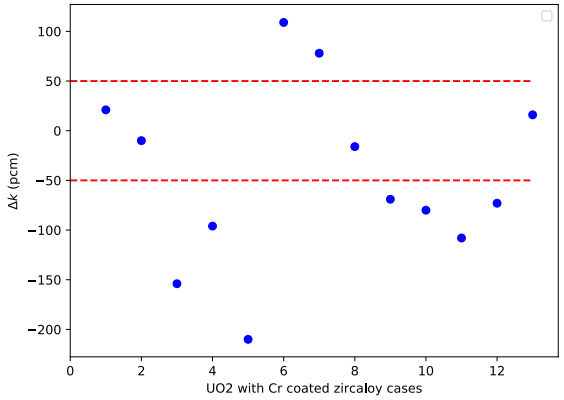

(c) Coating homog-3

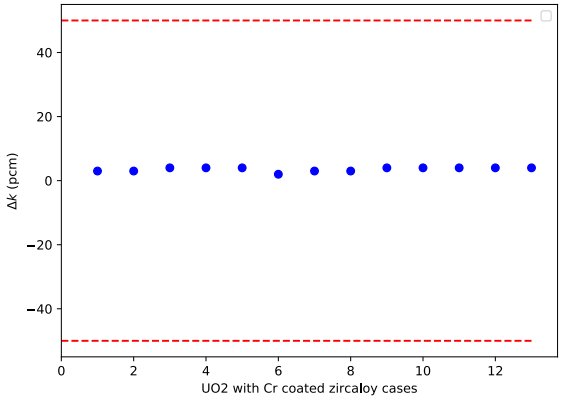

(d) Coating homog-4

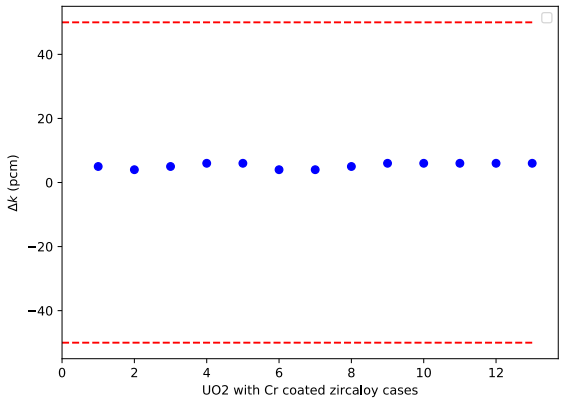

(e) Coating homog-5

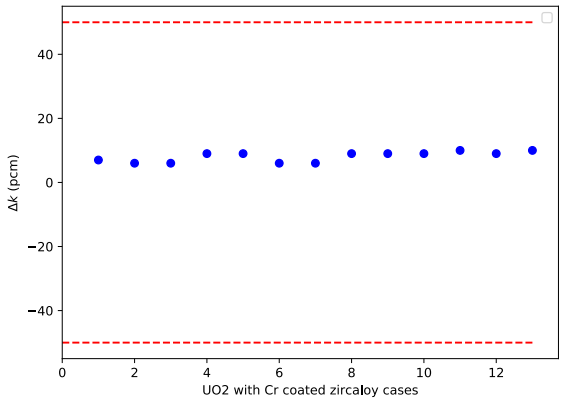

(f) Coating homog-6

Figure 1. k_{inf} differences for Cr coat model.

3.2 FECRAL INVESTIGATION

A standard GE14 DOM type BWR lattice was used for this study. General design parameters for the modeled lattice are provided in Table 10. Lattices with Zircaloy-2 and FeCrAl clad were depleted up to 80 GWd/MTU. Comparison of lattice k_{inf} with burnup are shown in Figure 2.

Table 10. GE14 lattice parameters

Parameter	Value
Lattice type	GE14-DOM
Highest ^{235}U enrichment	4.90%
Lowest ^{235}U enrichment	1.60%
Gad loading	3%-8%
Nominal case clad type	Zircaloy-2
FeCrAl clad type	Fe 75% Cr 20% Al 5%
Void fraction	40%
Fuel temperature (K)	900
Coolant temperature (K)	560

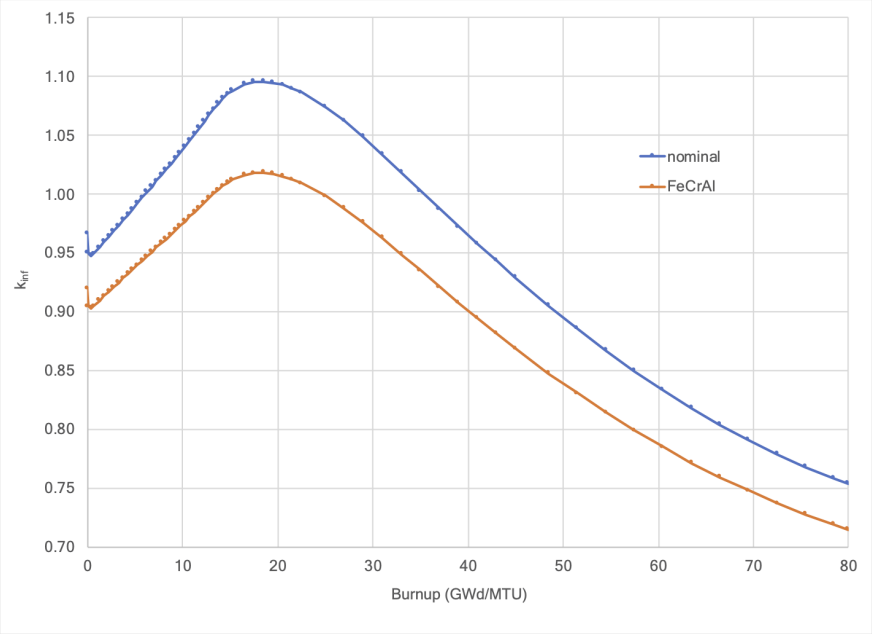

Figure 2. Comparison of BWR lattice k_{inf} with Zircaloy-2 cladding to FeCrAl cladding.

Depletion calculations for GE14 lattice with FeCrAl clad results in lower k_{inf} values compared to Zircaloy-2 clad. The difference in $k_{inf}$is around 470 pcm at BOL. The difference in k_{inf} is reduced to 390 pcm at the end of life (EOL).

The effect of ^{235}U enrichment on the end of cycle reactivities for the first (12–15 GWD/MTU) and second cycles (24–30 GWD/MTU) were tested for the FeCrAl clad lattice. ^{235}U enrichment of each fuel pin was

increased by 5, 10, and 50%, and the results are plotted in Figure 3. The highest fuel pin enrichment for these cases is respectively 5.15%, 5.39%, and 7.35%.

As seen in Figure 3, even a 10% increase in ^{235}U enrichment is not adequate to meet first-cycle reactivity. An increase of more than 25% in ^{235}U enrichment is required to meet the end of cycle (EOC) reactivity.

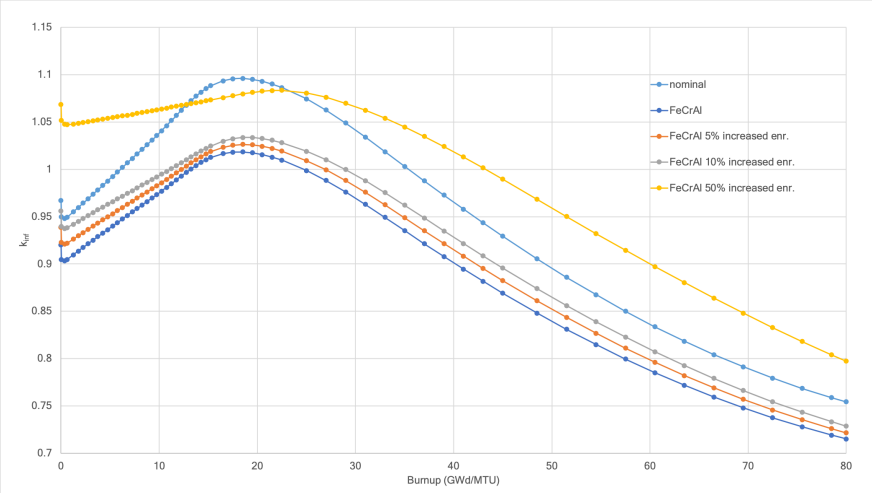

Figure 3. Comparison of BWR lattice k_{inf} with FeCrAl cladding with varying ^{235}U enrichment.

In an attempt to match EOC reactivity, pin radius is increased and clad thickness is reduced while maintaining a constant gap thickness. Figure 4 illustrates the effect of 50% reduction in clad thickness (and the increase in pin radius by the same amount) for the FeCrAl clad lattice. A combination of 10% increase in ^{235}U enrichment and reduced clad thickness was also tested, and the k_{inf} trend is included in Figure 4. This study shows that FeCrAl lattices will require significant design changes (i.e., a combination of ^{235}U enrichment increase, clad thickness decrease, or fuel radius increase), to produce similar k_{inf} curves as in current UO_2-Zry fuel. For this reason, an optimized FeCrAl lattice design that was generated in this study was used as described in Section 2 for benchmark identification studies.

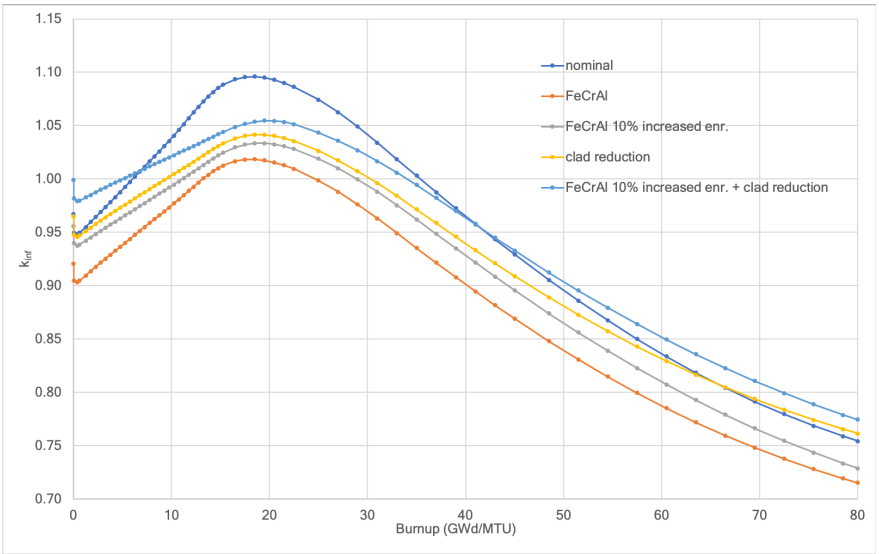

Figure 4. Comparison of BWR lattice k_{inf} with FeCrAl cladding with varying design changes.

3.3 SILICIDE FUEL INVESTIGATION

Preliminary studies comparing CE-KENO, Shift and Polaris results for U_3Si_2 fuel in the WEC 17×17 PWR assembly indicate a difference of more than 300 pcm between Polaris and KENO results, while CE-KENO and Shift results agree. Good agreement between NEWT and MC codes prompted further analysis of Polaris results. To simplify the problem, the pin cell model specified in the WEC 17×17 lattice with the same fuel rod specifications was used for the analysis. Specifications of the pin cell that was used in this study are provided in Table 11.

Table 11. PWR pin cell used for U_3Si_2 fuel investigation

Parameter	Value
Pin pitch	1.26
Fuel pin radius	0.4096
Clad inner radius	0.418
Clad outer radius	0.475
^{235}U enrichment	4.20
Clad material	Zircaloy-4

The pin cell problem shows discrepancies similar to those with CE-KENO and NEWT results as the lattice model. A series of PWR pin cell problems with incremental changes in material compositions were modeled. The results of these pin cell problems are summarized in Table 12. Case 1 represents the original pin cell problem, and the CE-KENO and NEWT results agree with less than 30 pcm difference, while Polaris and NEWT results show a bias of -332 pcm.

Table 12. Results of the U_3Si_2-fueled pin cell investigation

Case	Description	CE KENO	NEWT	Polaris	Polaris-NEWT
1	Base case U_3Si_2 fuel with SiC clad	1.26548	1.26520	1.26188	-332
2	U_3Si_2 fuel with Zircaloy-4 clad		1.25537	1.25318	-218
3	U_3Si_2 fuel with Si clad		1.26694	1.26362	-331
4	U_3Si_2 fuel with clad volume replaced by He		1.27274	1.26920	-353
5	U (U_3Si_2 fuel with Si removed) with SiC clad	1.27632	1.27585	1.27272	-312
6	U (with 4.9% ^{235}U enrichment) with SiC clad		1.20442	1.20271	-171
7	UO_2 fuel with SiC clad		1.24469	1.24381	-88

SiC clad was replaced with Zircaloy-4 clad for Case 2. A reduction of more than 100 pcm in the Case 1 bias raised questions about how SiC clad was treated in Polaris. However, Si-only cladding in Case 3 and He-only cladding (clad is removed and the volume is replaced by gap) in Case 4 show biases similar to the Case 1 bias. Case 4 shows that, there is a negative bias introduced by Zircaloy-4 clad which reduces the bias introduced by U_3Si_2fuel. In other words, more than 100 pcm of the original bias (≈330 pcm) originates from lack of Zircaloy-4 clad.

The source of the remaining bias was investigated in the fuel composition of Case 1. When Si was removed from the fuel (Case 5), the results show that Si does not have a significant effect on the bias. Moreover CE-KENO and NEWT results agree (62 pcm) for the metallic fuel used in Case 5.

Uranium isotope distributions and number densities were compared between uranium in UO_2 and U_3Si_2 fuels (provided in Table 13). Although ^{238}U and ^{236}U number densities are similar, the ^{235}U number density

is roughly 60% larger in U_3Si_2. If the uranium isotope number densities in UO_2 are used, then the bias for the metallic fuel is reduced by 140 pcm (Case 6). As seen in the last pin cell test case, oxygen was added to the metallic fuel specified in Case 6, effectively modeling UO_2 fuel with SiC clad. Case 7 shows that adding oxygen to fuel reduces the bias by more than 80 pcm.

Table 13. Comparison of U isotope concentrations (atoms/barn-cm) in U_3Si_2 and UO_2 fuel

Isotope	U_3Si_2	UO_2
^{234}U	1.01E-05	6.52E-06
^{235}U	1.15E-03	7.30E-04
^{236}U	5.29E-06	3.34E-06
^{238}U	2.60E-02	2.25E-02

Summary:

- NEWT results do not show the large k_{eff} difference seen in Polaris results compared to the reference CE-KENO results.
- Si in fuel has a negligible effect on bias.
- Use of SiC clad instead of Zircaloy-4 clad introduces more than -100 pcm.
- ^{235}U number density in U_3Si_2 is 60% larger than ^{235}U number density in 4.9% enriched UO_2 fuel. This difference causes -140 pcm difference in k_{inf}.
- Including oxygen in the fuel reduces the bias by more 80 pcm.

The reduction in bias with Zircaloy-4 clad and inclusion of oxygen to fuel is considered to be due to the heterogeneous f-factors (self-shielding factors) used in Polaris cross section processing. As the pin compositions become more consistent with the pin cell model used to calculate f-factors, the bias decreases. Comparison of NEWT results using CENTRM and BONAMI cross section processing modules for Case 1 and Case 7 show that the bias between NEWT(CENTRM) and NEWT(BONAMI) results increases more than 100 pcm when U_3Si_2 fuel is used instead of UO_2 fuel (Table 14). The NEWT (BONAMI) sequence uses the same self-shielding factors as those used in Polaris. The self-shielding factors are generated using the AMPX IRFFACTOR module. IRFFACTOR generates self-shielding factors based on a set of reference continuous-energy unit cell calculations. The accuracy of the IRFFACTOR calculation can be improved with future methods enhancements and group structure optimization.

Table 14. Comparison of k_{inf} for CENTRM and BONAMI for U_3Si_2 and UO_2 fuel

	NEWT(BONAMI)	NEWT(CENTRM)	Difference
UO_2-SiC	1.24054	1.24527	-473
U_3Si_2-SiC	1.26075	1.26660	-585

3.4 CLAD DEPLETION EFFECT

For UO_2-Zry lattices, a common modeling assumption is to neglect clad depletion effects because of their small impact on lattice k_{inf} as a function of burnup. For ATF lattices, this assumption is revisited due to the larger absorption cross section of Cr isotopes compared to Zirconium isotopes. A simple depletion study was performed to compare the reactivity impact of clad depletion for Cr-coated cladding in a PWR lattice

and FeCrAl cladding in a BWR lattice. Each lattice was depleted, with and without clad depletion enabled, at HFP conditions to 60 GWD/MTU. Cycle-averaged boron was used for the PWR lattice, and a 40% void fraction was used for the BWR lattice. Table 15 shows the impact on k_{inf} as a function of burnup for both standard UO_2-Zry lattices and ATF lattices. The maximum reactivity increase is less than 35 pcm in all cases tested. Therefore, the clad depletion effect can be ignored in the test results.

Table 15. Impact of clad depletion on lattice k_{inf} as a function of burnup

Burnup (GWD/MTU)	PWR UO_2-Zry Δk (pcm)	PWR ATF[a] Δk (pcm)	BWR UO_2-Zry Δk (pcm)	BWR ATF[b] Δk (pcm)
0	0	0	0	0
10	25	29	22	6
20	26	33	30	16
30	24	32	25	20
40	20	29	19	26
50	15	27	14	29
60	12	24	10	33

[a] UO_2 fuel and Cr-coated cladding
[b] UO_2 fuel and FeCrAl cladding

4. POLARIS CODE ASSESSMENTS

This section focuses on code-to-code comparisons of calculated QOIs against high-fidelity reference CE MC calculations. Subsection 4.1 focuses on PWR ATF code assessments, Subsection 4.2 summarizes BWR ATF code assessments, and Subsection 4.3 presents an investigation of depletion uncertainty analysis.

4.1 PWR ATF CODE ASSESSMENTS

The comparisons in this section are based on the Westinghouse 4-loop 17×17 fuel design. An identical 2D quarter lattice was modeled both in Polaris and in CE Shift with reflective boundary conditions to represent infinite lattice, as shown in Figure 5. Five ATF designs are considered and compared to the standard UO_2 fuel with Zircaloy-4 clad design. Detailed specifications about the PWR ATF designs are provided in Table 16.

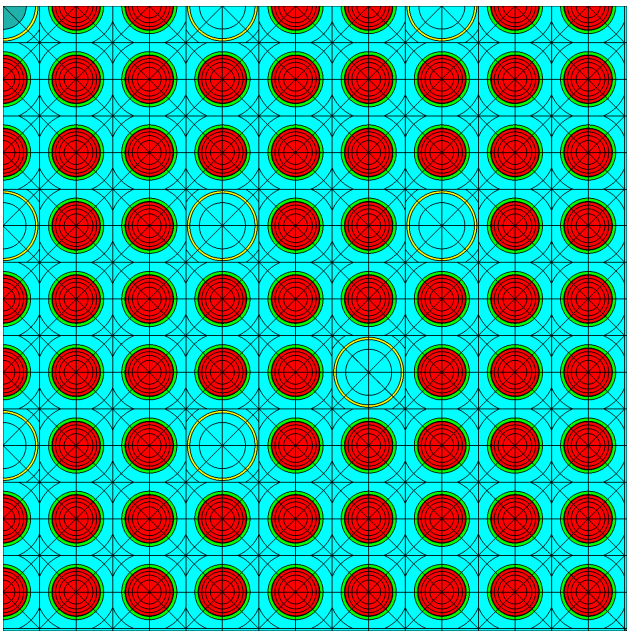

Figure 5. Westinghouse 4-loop 17×17 lattice model

Table 16. PWR ATF designs

Fuel	Clad	Enrichment %	Fuel density (g/cm^3)	Al_2O_3 (ppm)	Cr_2O_3 (ppm)	Cr-coat (μm)
UO_2 (Baseline)	Zircaloy-4	4.0	10.3			
Al_2O_3-Cr_2O_3 doped UO_2	Cr-coated Zircaloy-4	4.0	10.3	500	200	30
Cr_2O_3 doped UO_2	Cr-coated M5	4.0	10.3		1000	30
Cr_2O_3 doped UO_2	SiC	4.0	10.3		1000	
U_3Si_2	SiC	4.0	11.4			
U_3Si_2	Cr-coated Zircaloy-4	4.0	11.4			30

The lattice physics QOIs include k_{inf}, p, ϵ, (reproduction factor * thermal utilization factor) (η*f), ϕ_1/ϕ_2, Doppler temperature coefficient (DTC), moderator temperature coefficient (MTC), differential boron worth

(DBW), and control rod worth (CRW). The reactivity coefficients—boron and rod worth—are derived from the branch cases listed in Table 17.

Table 17. Branch cases

Branch number	Control rod position	Moderator temperature (K)	Moderator density (g/cm^3)	Boron concentration (ppm)	Fuel temperature (K)
1[a]	Out	585	0.70045	600	800
2	Out	585	0.70045	0	800
3	Out	293	1.00000	1,200	293
4	In	293	1.00000	1,200	293
5	Out	615	0.60811	0	800
6	Out	615	0.60811	600	800
7	Out	615	0.60811	1,200	800
8	Out	585	0.70045	1,200	800
9	Out	585	0.70045	600	1600
10	In	585	0.70045	0	800
11	In	585	0.70045	600	800
12	In	585	0.70045	1,200	800

[a] Reference condition for k_{inf} and four-factor formula assessments.

The lattice physics QOIs were computed as a function of fuel burnup. The base Polaris inputs were depleted at the following burnup points in GWD/MTU:

$$\{0, 0.1, 0.5, 1, 2, 4, 6, 8, 10, 12.5, 15, 17.5, 20, 25, 30, 35, 40, 45, 50, 55, 60, 65, 70, 75, 80\}$$

4.1.1 COMPARISONS WITH CE MONTE CARLO

From the base Polaris burnup data, 10 burnup points were chosen for Shift and Polaris comparison. A total of 60 Polaris restart inputs were created at each burnup point, along with a total of 720 Shift restart inputs at each burnup point for every branch case. All Shift calculations are converged to a maximum of 12 pcm uncertainty in k_{inf}. Each ATF design was depleted in Shift and Polaris at a constant specific power of 38.4 MW/MTU. The 10 burnup points in GWD/MTU are:

$$\{0, 0.1, 10, 20, 30, 40, 50, 60, 70, 80\}$$

All the QOI comparisons are given via three graphs (a) Base Polaris, (b) Difference between the ATF design and the standard UO_2-Zry design, and (c) Difference between Polaris and Shift.

Target accuracy for the QOIs is given as follows:

- 200 pcm difference in k_{inf}
- 400 pcm difference in four factors
- 0.25 difference in fast to thermal energy group flux ratio
- 5% difference in CRW
- 4 pcm/k difference in MTC
- 0.5 pcm/k difference in DTC
- 1 pcm/ppm difference in DBW

The target accuracy for k_{inf} and four-factor terms was based on the acceptance criteria in the previous LWR code assessment work (Mertyurek et al. 2017). The target accuracy for MTC and DTC were selected based on personal communications with experts, as well as MTC and DTC uncertainties that were estimated for a conventional PWR AP1000 17×17 fuel model using the Monte Carlo code Serpent (Shapiroa and Fratonib 2016). The target accuracies for the remaining QOIs were selected based on personal communications with experts in the field.

4.1.1.1 k_{inf} four-factor formula, and flux ratio comparison

The infinite multiplication factor k_{inf} can be expressed in terms of four factors: (1) the reproduction factor (η), (2) the thermal utilization factor (f), (3) the resonance escape probability (p), and (4) the fast fission factor (ϵ). Based on two-group diffusion theory, the four factors may be calculated from Polaris and Shift .*t*16 outputs as follows:

$$\eta * f = \frac{\nu\Sigma_{f2}}{\Sigma_{a2}} \tag{1}$$

$$p = \frac{\tilde{\Sigma}_{s1\to2}}{\tilde{\Sigma}_{R1}} \tag{2}$$

$$\epsilon = 1 + \frac{\nu\Sigma_{f1}}{\nu\Sigma_{f2}} \frac{\Sigma_{a2}}{\tilde{\Sigma}_{s1\to2}} \tag{3}$$

where

$$\tilde{\Sigma}_{s1\to2} = \Sigma_{s1\to2} - \Sigma_{s2\to1}\frac{\phi_2}{\phi_1}$$
$$\tilde{\Sigma}_{R1} = \Sigma_{a1} + \tilde{\Sigma}_{s1\to2}.$$

Figure 6 through Figure 10 show ATF lattice comparisons of burnup-dependent values of k_{inf}, η*f, p, ϵ, and ϕ_1/ϕ_2, respectively. Two major physical phenomena are exhibited in these figures: the hardened spectrum of U_3Si_2 fuel and the reduced reactivity of the Cr-coated cladding.

As shown in Figure 10(b), U_3Si_2 fuel has a harder spectrum than UO_2 fuel. This is due to the higher uranium density in the fuel volume (i.e., smaller moderator-to-fuel ratio) and also due to the reduced internal moderating power of Si compared to O. The hardened spectrum of U_3Si_2 leads to larger ϵ, as shown in Figure 9(b), and smaller p, as shown in Figure 8(b).

The second major effect is the reduced reactivity of Cr-coated cladding. The Cr-coated cladding leads to more thermal neutron absorption. This leads to smaller η*f values. Furthermore, this effect hardens the neutron spectrum which increases ϕ_1/ϕ_2, increases ϵ, and decreases p, but not to the same degree as the U_3Si_2 fuel composition. The net effect of the Cr-coated cladding is a decrease in k_{inf} as compared to standard Zircaloy cladding.

Figure 6(c) through Figure 10(c) provide comparisons of k_{inf}, η*f, p, ϵ, and ϕ_1/ϕ_2 between Polaris and Shift at 10 burnup points. At each burnup step, the differences between Polaris and Shift were calculated as (Polaris results - Shift results). Thus, a negative value means that Polaris is underpredicting, and a positive value means that Polaris is overpredicting in comparison to the reference Shift results. Both η*f and ϵ values are overpredicted, while the p values are underpredicted. Overall, the k_{inf} values are underpredicted. The

U_3Si_2 fuel cases have the the largest difference in k_{inf} ranging from about 250–350 pcm. This underprediction is explained in Section 3.3 and requires future enhancements to IRFFACTOR to produce more accurate self-shielding factors. The Polaris predictions for UO_2 based fuel dips below the target accuracy criteria at high burnups. This behavior is common for UO_2-Zry and ATF cases and is consistent with previous work in (Mertyurek et al. 2017).

4.1.1.2 Moderator temperature coefficient comparison

The reactivity is defined as $\rho = \frac{k-1}{k}$, which measures the deviation from a critical core. The reactivity worth is defined as the difference of reactivity induced to the core:

$$\begin{aligned} \Delta\rho &= \frac{k_1 - 1}{k_1} - \frac{k_2 - 1}{k_2} \\ &= \frac{k_1 - k_2}{k_1 k_2} \end{aligned} \tag{4}$$

The MTC is defined as the reactivity worth per degree change in moderator temperature. MTC values have strong dependence on the moderator-to-fuel ratio and the moderator boron content. Compared to standard UO_2-Zry fuel, U_3Si_2 fuel has a higher heavy metal density. In return, U_3Si_2 fuel has a lower moderator-to-fuel ratio and thus a lower MTC. The MTC comparisons at 0 ppm, 600 ppm, and 1,200 ppm are shown in Figures 11, 12, and 13. The MTCs at 0 ppm, 600 ppm, and 1200 ppm are negative across all burnup points.

Figures 11(c), 12(c), and 13(c) show differences in Polaris MTC compared to Shift MTC. The differences increase in magnitude as burnup increases due to the accumulation of fission products and actinides in the fuel. At all burnup points, the MTC differences are within the target 4 pcm/K criteria.

4.1.1.3 Control rod worth comparison

The *control rod worth* is defined as the reactivity worth caused by control insertion. The total control rod worth is the reactivity difference between all control rods fully withdrawn from the core and all control rods fully inserted. For the same amount of neutron-absorbing medium, the control rods have less effect for U_3Si_2 fuel compared to standard UO_2-Zry again due to the higher heavy metal density in U_3Si_2 fuel. The CRW comparisons at 293 K 1,200 ppm, 585 K 0 ppm, 585 K 600 ppm, and 585 K 1,200 ppm are shown in Figures 14, 15, 16, and 17. The CRW results from Polaris and Shift agree very well. The differences meet the target 5% criteria.

4.1.1.4 Doppler temperature coefficient comparison

The *Doppler coefficient* is defined as the change in reactivity per degree change in the fuel temperature. This is one of the most important coefficients due to its immediate response to the change in fuel temperature. The Doppler coefficient is always negative. Compared to standard UO_2-Zry fuel, U_3Si_2 fuel DTC is worth less (less negative) at low burnups, and it is worth more (more negative) at high burnups. Increasing fuel temperature hardens the flux spectrum. At low burnups, the softer spectrum of UO_2fuel compared to U_3Si_2 fuel is more sensitive to increasing fuel temperature. Overall, the Polaris and Shift difference in DTC is small and meets the target 0.5% pcm/K criteria shown in Figure 18(c).

4.1.1.5 Differential boron worth comparison

Differential boron worth is defined as the change in reactivity per unit change in boron concentration. Due to the higher uranium density in U_3Si_2 fuel volume, the boron is worth less (less negative) for U_3Si_2 fuel compared to standard UO_2-Zry fuel. The DBW results from Polaris and Shift are almost identical, as shown in Figure 19(c). The differences are well below the target 1 pcm/ppm criteria.

4.1.1.6 Effective delayed neutron fraction and precursor decay constant comparison

Figure 20 shows the effective delayed neutron fraction (β) for all ATF designs. The β for ATF designs are similar and in line with the typical UO_2-Zry fuel. The β for U_3Si_2 fuel is increased by less than 1% at all burnup points. From Figure 21, it should be noted that the precursor decay constant (λ) for U_3Si_2 fuel is increased by roughly 1.3%. From the same figures—20 and 21—the fuel dopant has little impact on β and λ.

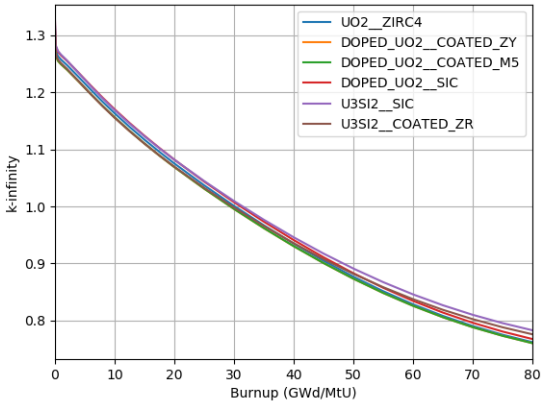

(a) Polaris base

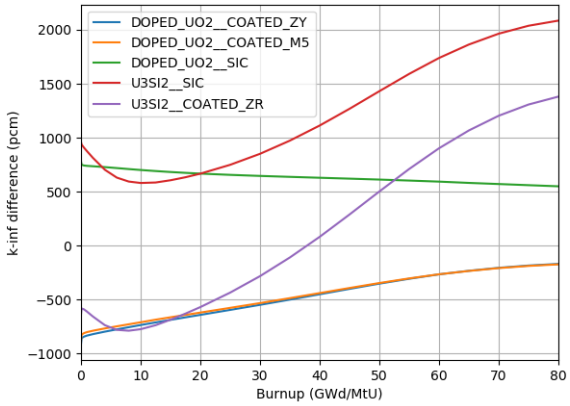

(b) Diff ATF to UO_2/Zirc-4

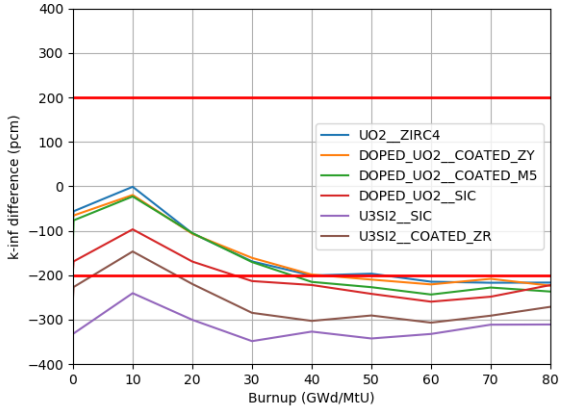

(c) Diff Polaris to Shift

Figure 6. k_{inf} comparison.

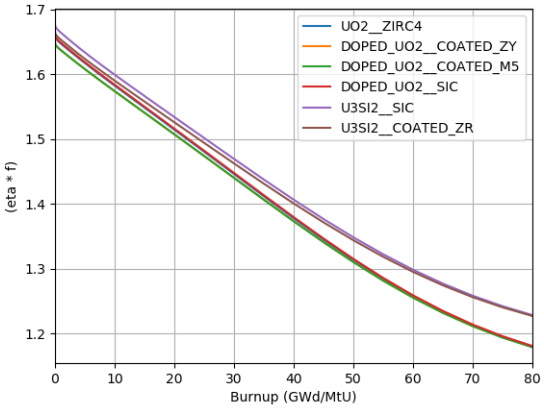

(a) Polaris base

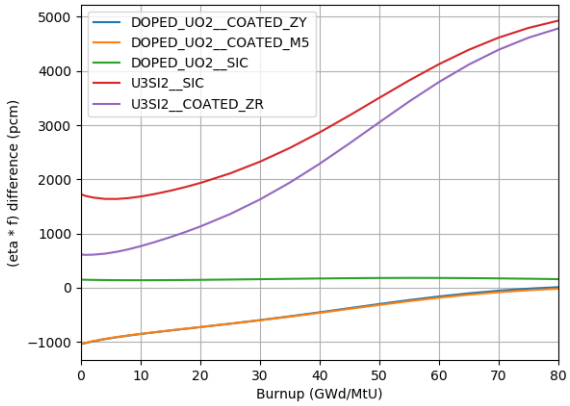

(b) Diff ATF to UO_2/Zirc-4

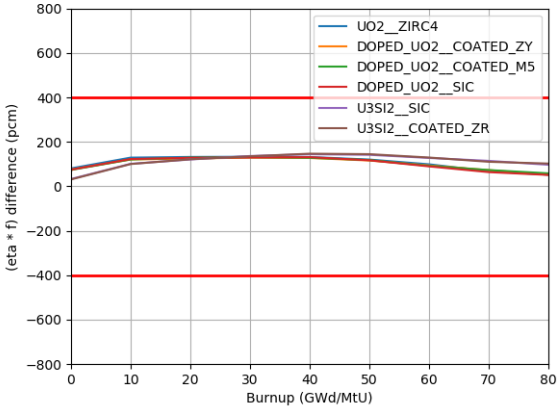

(c) Diff Polaris to Shift

Figure 7. Reproduction factor (η) * the thermal utilization factor (f) comparison.

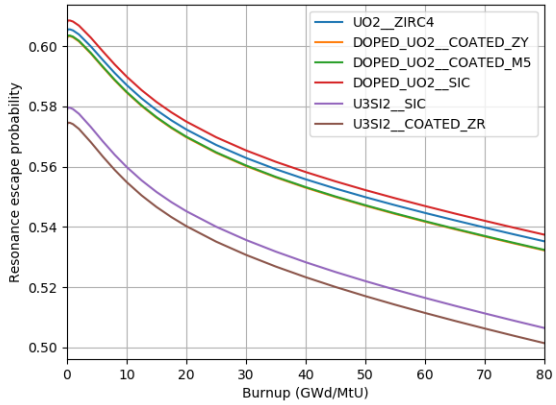

(a) Polaris base

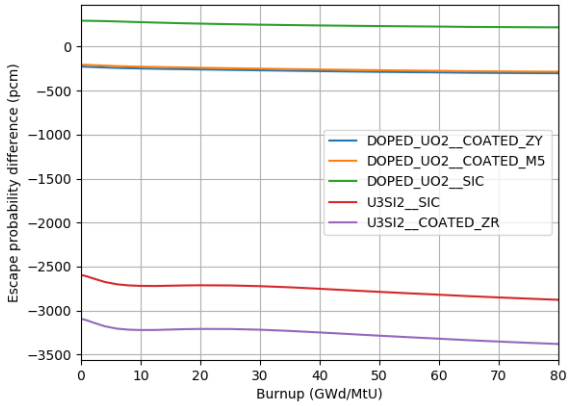

(b) Diff ATF to UO_2/Zirc-4

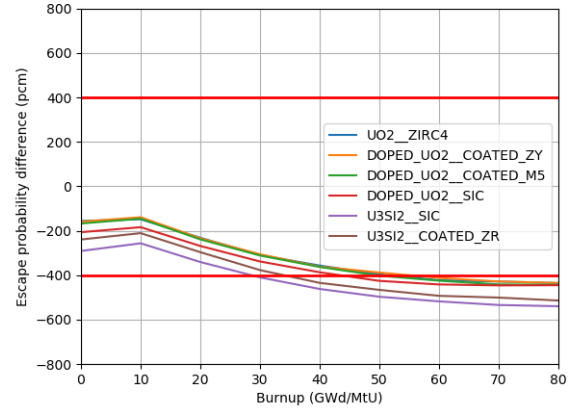

(c) Diff Polaris to Shift

Figure 8. Resonance escape probability (p) comparison.

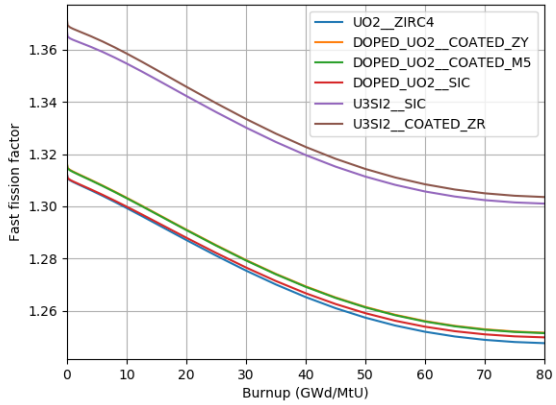

(a) Polaris base

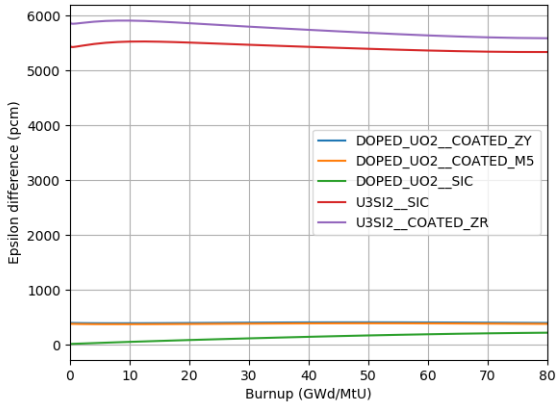

(b) Diff ATF to UO_2/Zirc-4

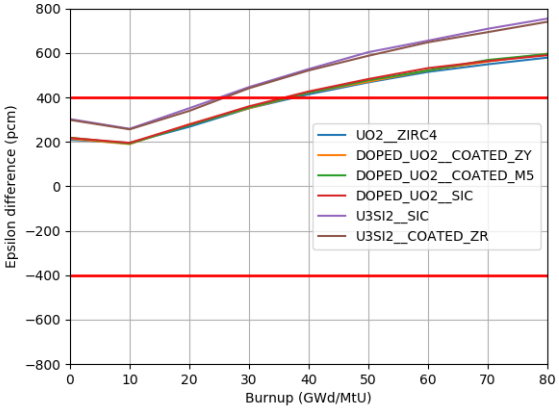

(c) Diff Polaris to Shift

Figure 9. The fast fission factor (ϵ) comparison.

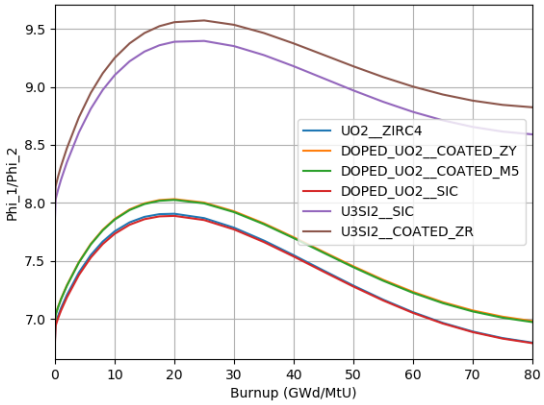

(a) Polaris base

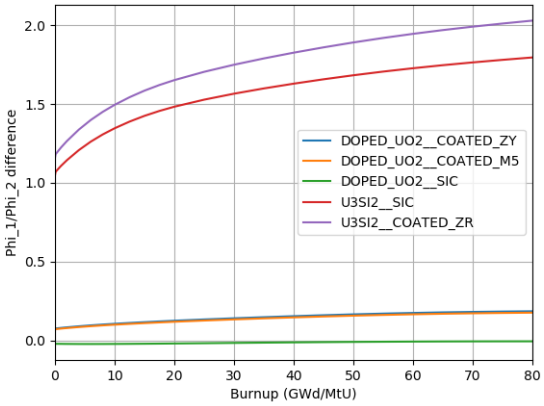

(b) Diff ATF to UO_2/Zirc-4

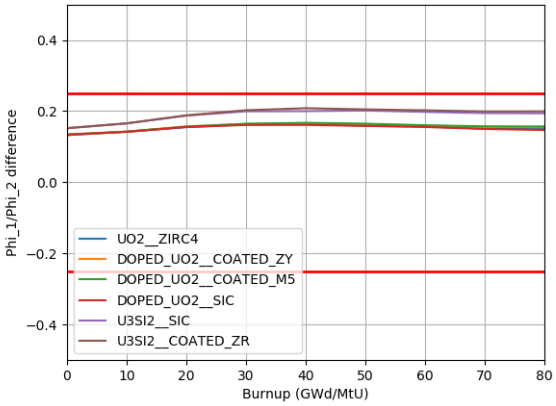

(c) Diff Polaris to Shift

Figure 10. Fast to thermal energy group flux ratio (ϕ_1/ϕ_2) comparison.

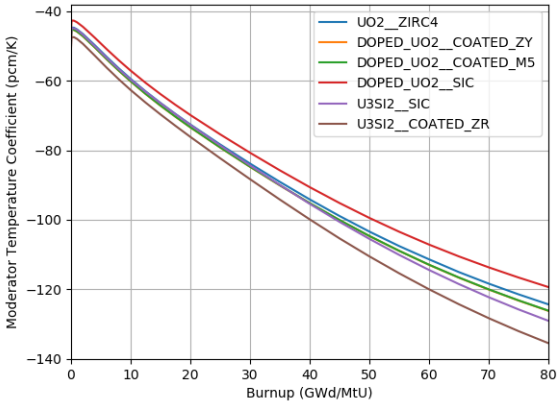

(a) Polaris base

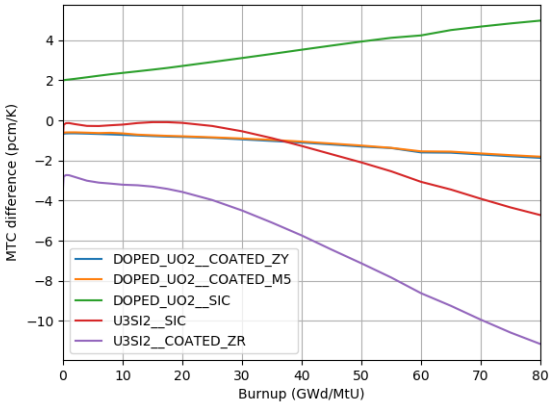

(b) Diff ATF to UO_2/Zirc-4

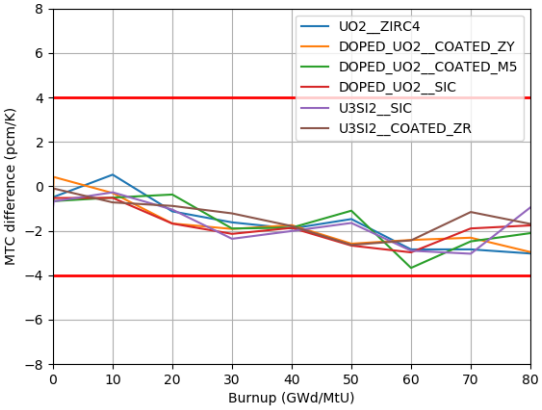

(c) Diff Polaris to Shift

Figure 11. MTC at 0 ppm comparison.

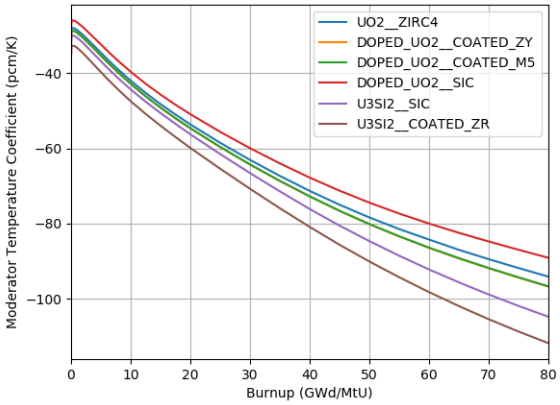

(a) Polaris base

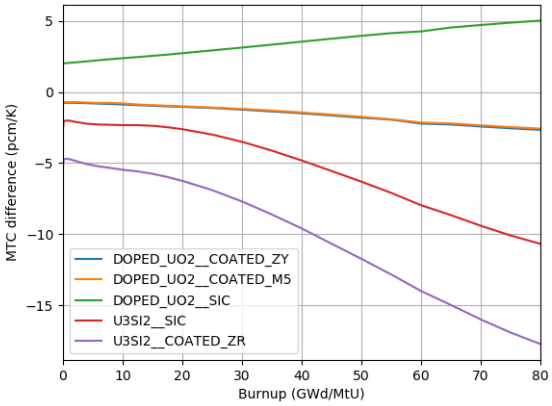

(b) Diff ATF to UO_2/Zirc-4

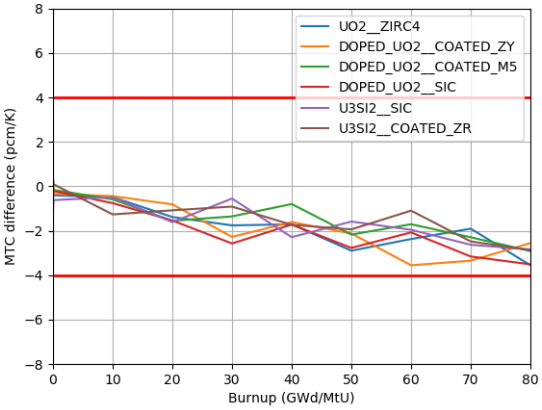

(c) Diff Polaris to Shift

Figure 12. MTC at 600 ppm comparison.

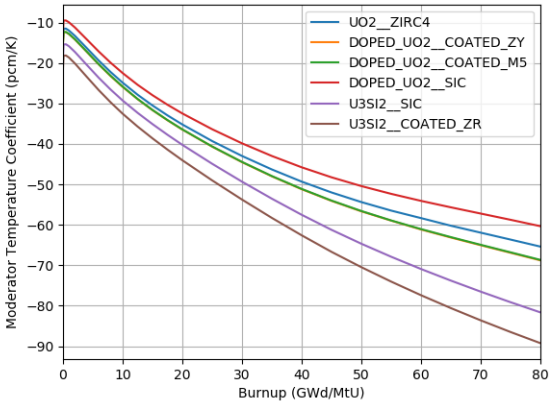

(a) Polaris base

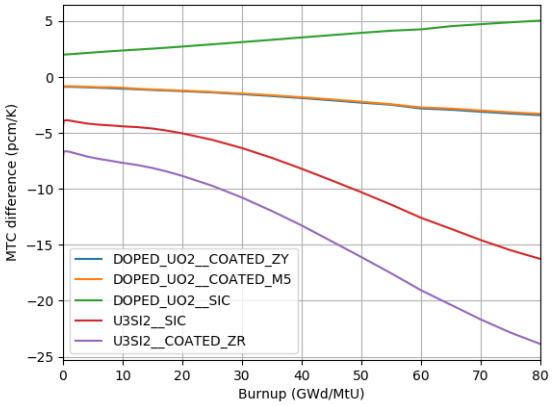

(b) Diff ATF to UO_2/Zirc-4

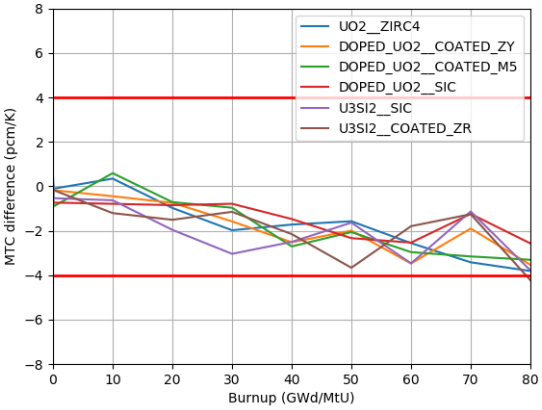

(c) Diff Polaris to Shift

Figure 13. MTC at 1,200 ppm comparison.

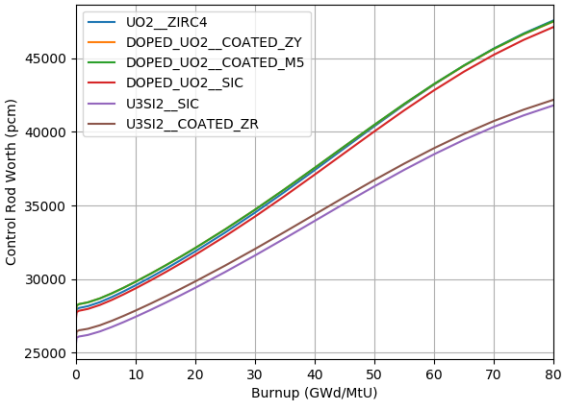

(a) Polaris base

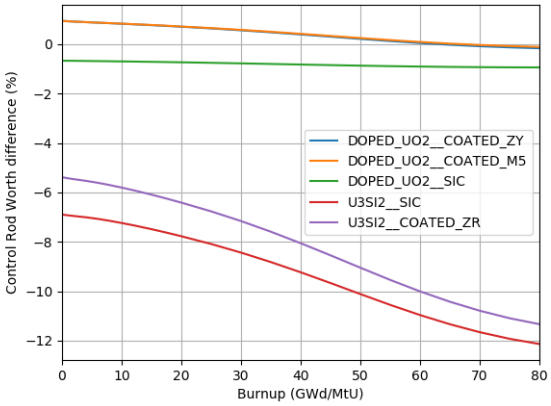

(b) Diff ATF to UO_2/Zirc-4

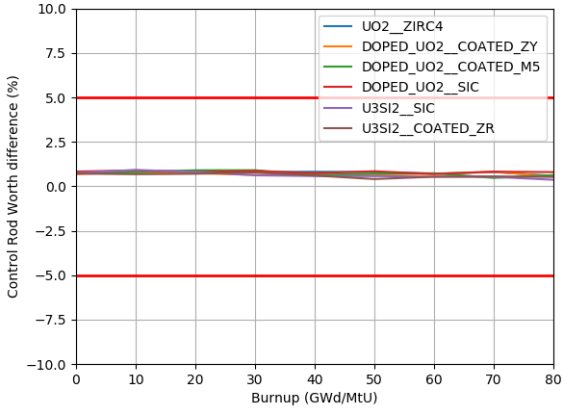

(c) Diff Polaris to Shift

Figure 14. CRW at 293 K 1,200 ppm comparison.

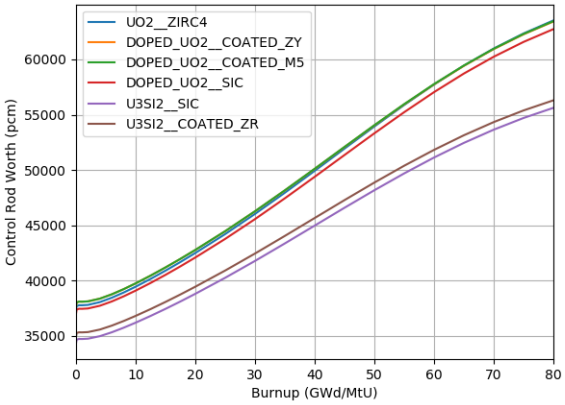

(a) Polaris base

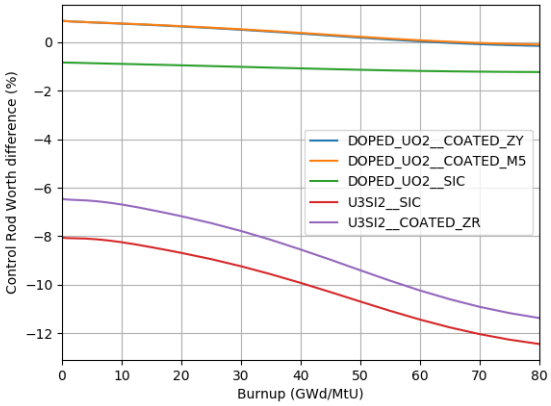

(b) Diff ATF to UO_2/Zirc-4

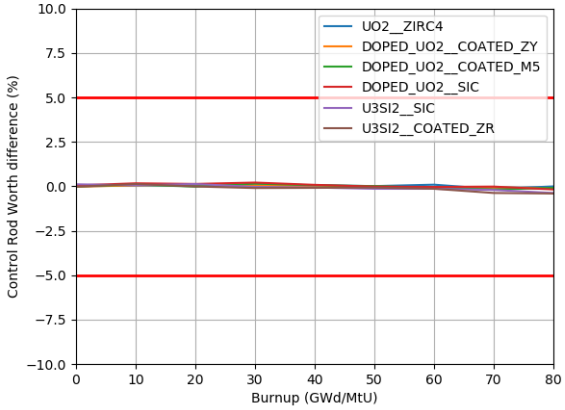

(c) Diff Polaris to Shift

Figure 15. CRW at 585 K 0 ppm comparison.

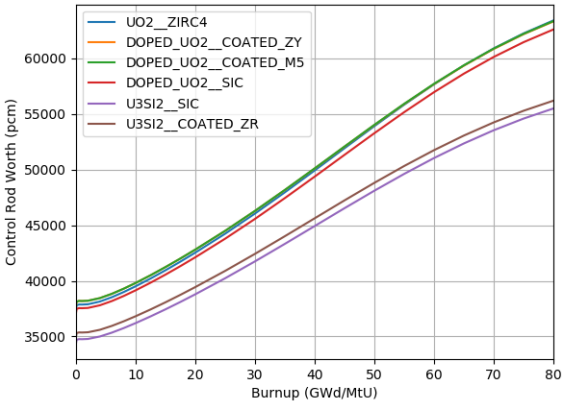

(a) Polaris base

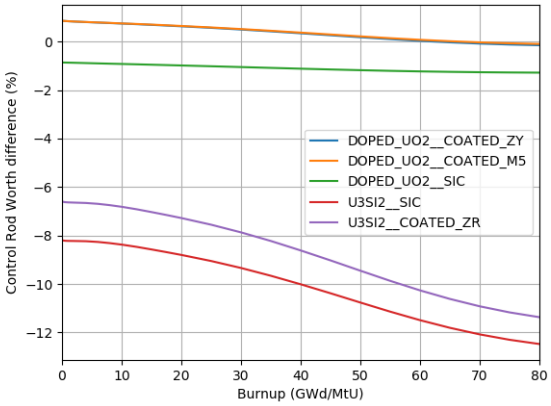

(b) Diff ATF to UO_2/Zirc-4

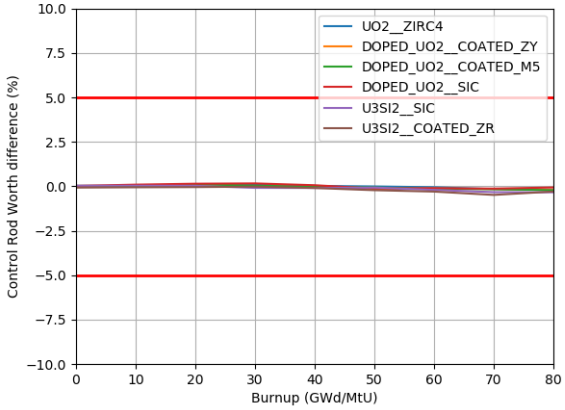

(c) Diff Polaris to Shift

Figure 16. CRW at 585 K 600 ppm comparison.

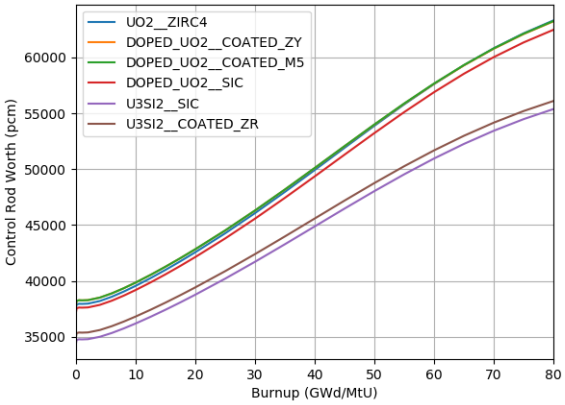

(a) Polaris base

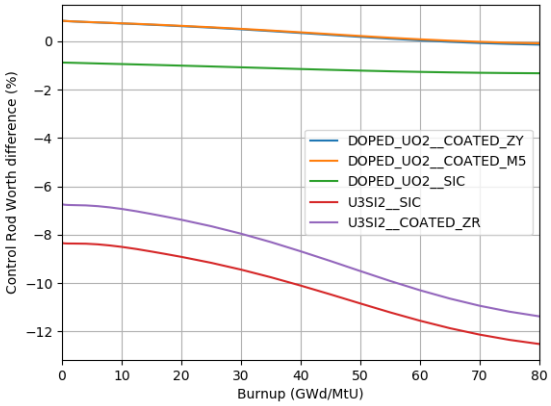

(b) Diff ATF to UO_2/Zirc-4

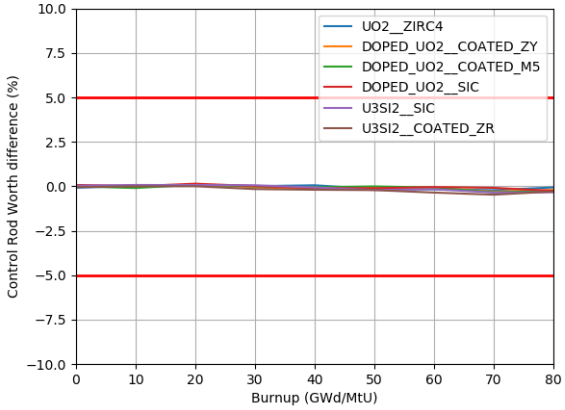

(c) Diff Polaris to Shift

Figure 17. CRW at mod 585 K 1,200 ppm comparison.

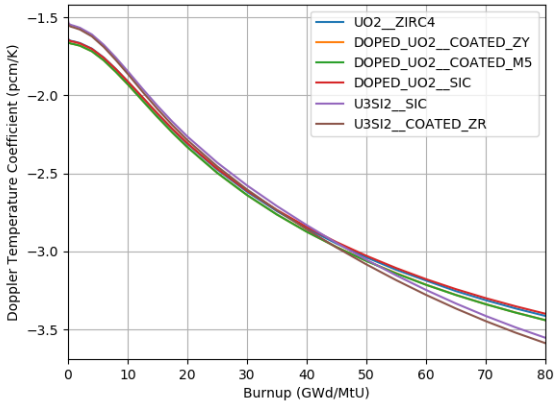

(a) Polaris base

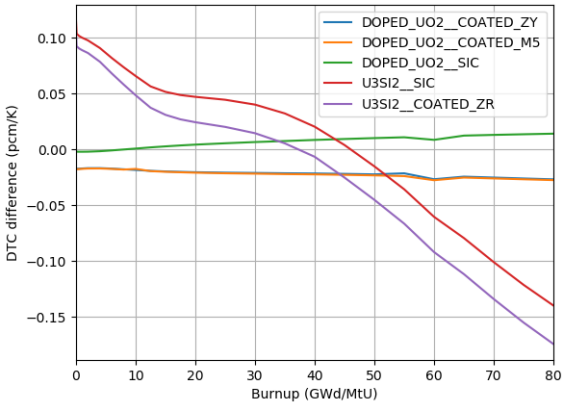

(b) Diff ATF to UO_2/Zirc-4

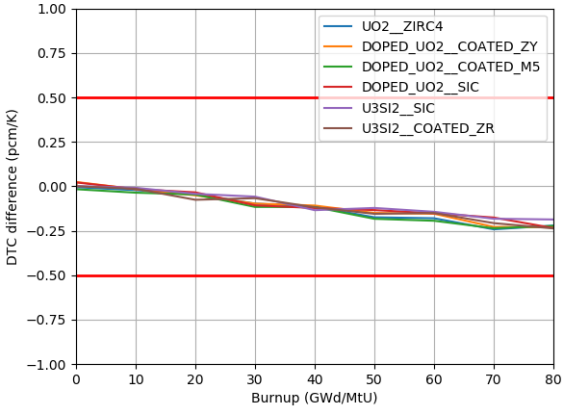

(c) Diff Polaris to Shift

Figure 18. DTC comparison.

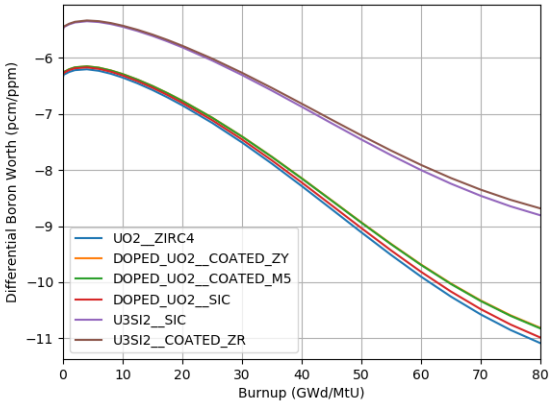

(a) Polaris base

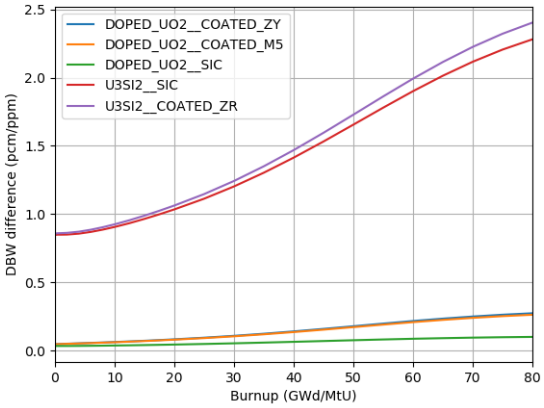

(b) Diff ATF to UO_2/Zirc-4

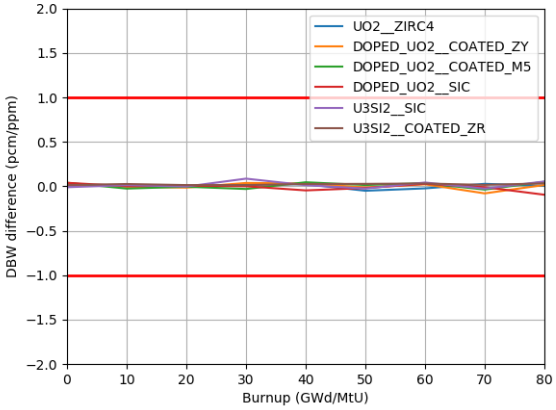

(c) Diff Polaris to Shift

Figure 19. DBW comparison.

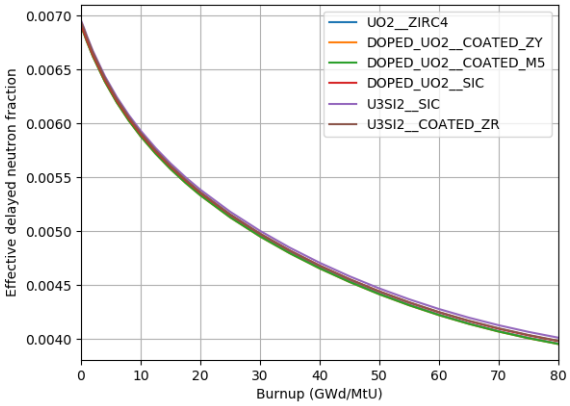

(a) Polaris base

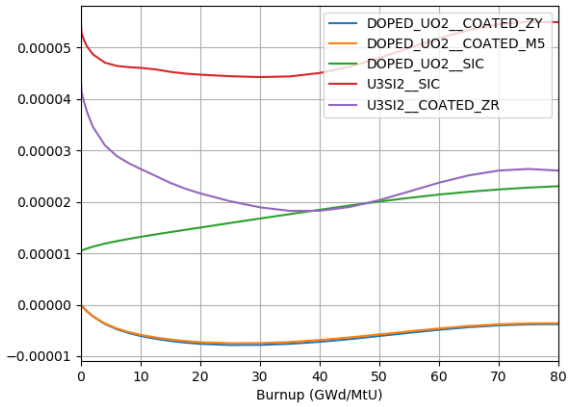

(b) Diff ATF to UO_2/Zirc-4

Figure 20. Effective delayed neutron fraction comparison for ATF designs.

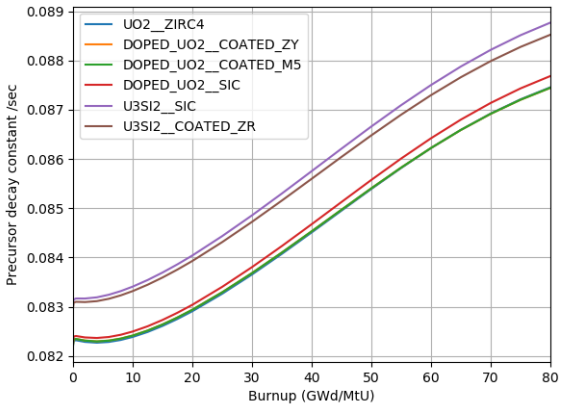

(a) Polaris base

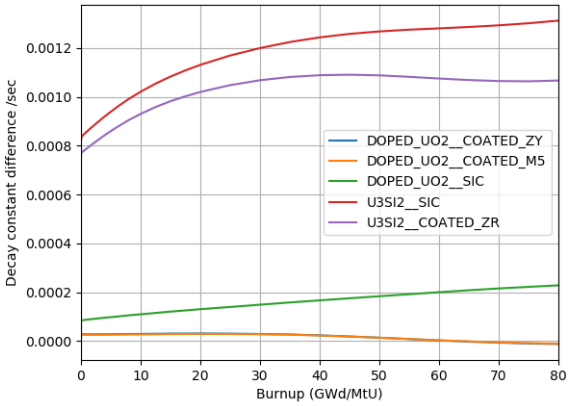

(b) Diff ATF to UO_2/Zirc-4

Figure 21. Decay constant comparison for ATF designs.

4.2 BWR ATF CODE ASSESSMENTS

Although the primary focus of this report has been PWR ATF code assessments, BWR ATF assessments have been investigated at BOL for GE14 10×10 and ATRIUM 11×11 lattices. Figure 22 shows the GE14 10×10. The ATRIUM 11×11 lattice is proprietary.

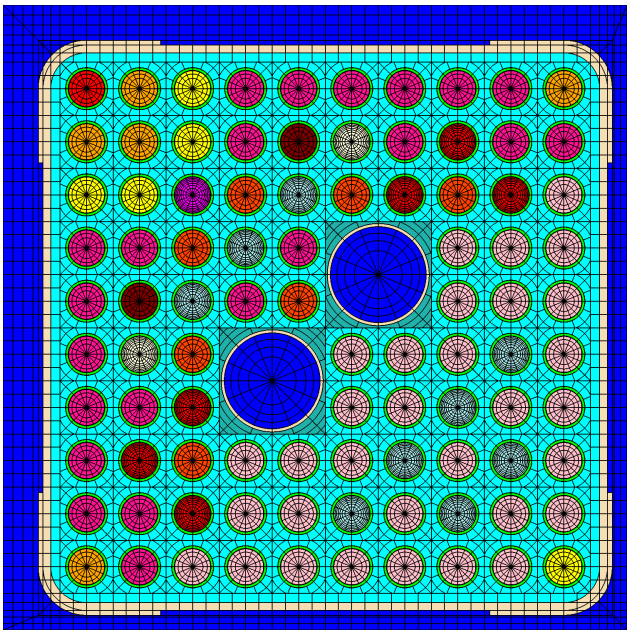

Figure 22. GE14 10×10 lattice model.

4.2.1 COMPARISONS WITH CE MONTE CARLO

Comparison of k_{eff} differences for CE KENO and Polaris are given in Table 18. The GE14 10×10 results are all within the 200 pcm target criteria, while the ATRIUM 11×11 results are just above the target accuracy.

Table 18. Comparison of k_{eff} for CE KENO and Polaris in BWR ATF designs

Fuel	Clad	CE KENO	Polaris	Difference (pcm)
GE14 10×10 UO_2 (Baseline)	Zircaloy-2	0.96307	0.96234	-73
GE14 10×10 UO_2	Cr-coated Zircaloy-2	0.96250	0.96197	-53
GE14 10×10 UO_2	FeCrAl	0.91585	0.91613	28
GE14 10×10 UO_2 (optimized)	FeCrAl	0.99488	0.99399	-89
ATRIUM 11×11 UO_2 (Baseline)	Zircaloy-2	1.42225	1.42022	-203
ATRIUM 11×11 Cr_2O_3 doped UO_2	Zircaloy-2	1.42188	1.41984	-204

4.3 DEPLETION UNCERTAINTY ANALYSIS

Sampler depletion uncertainty analysis was performed for selected BWR and PWR lattices to quantify uncertainty in k_{inf} due to nuclear data uncertainties. The Sampler sequence in SCALE is capable of perturbing nuclear data (cross sections, decay constants, and fission yields) based on stochastic samples of their respective uncertainties. Sampler can then automate Polaris depletion calculations for each set of perturbed data. The variation in the depletion results then provide a quantification of nuclear data uncertainties on the depletion results.

BWR and PWR lattices analyzed in this section are listed in Table 19. Figure 23 compares the k_{inf} trend and the associated uncertainty with depletion of BWR lattices at nominal conditions (40% void fraction). The Cr-coated Zircaloy-2 case agrees well with the nominal UO_2-Zry case and overlaps the curve. In order to compare uncertainties in the calculated k_{inf}, standard deviations are also plotted in Figure 24. The greatest uncertainties are observed at beginning of cycle (BOC), while the lowest uncertainties are located around gadolinium peaks. In general, FeCrAl cases exhibit greater uncertainties compared to the other two cases. The large uncertainties at BOC are due to gadolinium loadings. Gadolinium introduces additional uncertainty due to the uncertainty in cross sections. Gadolinium also hardens the spectrum, causing increased sensitivity to ^{238}U inelastic scattering. The largest component of the uncertainty contributed by gadolinium is caused by ^{157}Gd. ^{157}Gd depletes faster than ^{155}Gd, and the uncertainty reaches its minimum before the gadolinium peak. After ^{157}Gd is depleted, many competing reactivity effects—such as resonance, spatial self shielding, and spatially dependent Pu buildup—dominate the overall uncertainty (Jessee 2008) . After the gadolinium peak, actinide and fission product buildup with burnup causes an increasing trend in uncertainty with burnup.

FeCrAl cases have larger uncertainties compared to the base UO_2-Zry case due to Fe uncertainty in the clad. Optimized FeCrAl fuel has a larger pin diameter; therefore, there is more fuel contributing to the larger uncertainty at BOC compared to the original FeCrAl case.

Reasons for the inflection points seen in the standard deviation of k_{inf} in Figure 23 become clearer when k_{inf} trends for 10 representative samples generated by Sampler are plotted with the standard deviation of all samples in Figure 25. While the standard deviation reaches its minimum with depletion of ^{157}Gd, the steep increase in uncertainty is caused by a large variation in k_{inf} at the gadolinium peak.

As in BWR lattices, depletion analysis for the PWR lattices at nominal conditions (1,300 ppm boron) are shown in Figures 26 and 27. All PWR lattice cases exhibit the the same trend with depletion, and the k_{inf}

values are separated by small biases. U_3Si_2 fuel cases have higher k_{inf} and higher uncertainties compared to other cases. Separation among the cases is clearer in Figure 27. U_3Si_2 fuel has a slightly harder spectrum than the UO_2-Zry case, so the effect of increased sensitivity to ^{238}U cross sections (mainly in elastic scattering) is the main reason for the bias seen in uncertainties. Uncertainty in k_{inf} decreases with burnup until 30 GWd/MTU due to depletion of ^{235}U and ^{238}U, and it starts to increase again as actinides such as ^{239}Pu and fission products build up with burnup.

Figure 28 shows the standard deviation of all samples and k_{inf} trend with burnup for 10 representative samples generated by Sampler for the UO_2-Zry lattice. As shown in the figure, the large deviation in k_{inf} at BOC decreases until it reaches its minimum at around 30 GWd/MTU. The increase in standard deviation with burnup is also clear from the separation of k_{inf} trends for the samples after 30 GWd/MTU.

Table 19. Lattice types included in depletion uncertainty analysis

Case	Lattice type	Fuel	Clad
Chromium-coated Zirc	GE14	UO_2	Cr-coated Zircaloy-2
FeCrAl		UO_2	FeCrAl
FeCrAl-optimized dimensions		UO_2	FeCrAl
UO_2-Zirc clad		UO_2	Zircaloy-2
Cr_2O_3−M5	W 17×17	Cr_2O_3-doped UO_2	Cr-coated M5
UO_2-SiC		UO_2	SiC
Cr_2O_3−Al_2O_3−Zirc		Cr_2O_3−Al_2O_3-doped UO_2	Zircaloy-4
Cr_2O_3−UO_2−SiC		Cr_2O_3-doped UO_2	SiC
U_3Si_2−Cr-coated		U_3Si_2	Cr-coated Zircaloy-4
U_3Si_2−SiC		U_3Si_2	SiC

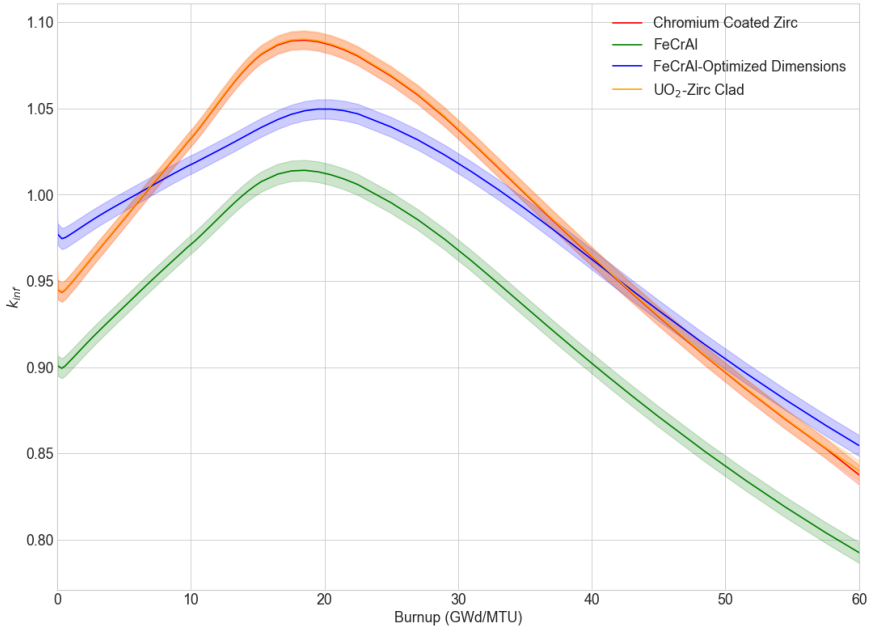

Figure 23. Comparison of BWR lattice k_{inf} with depletion at HFP and 40% void fraction.

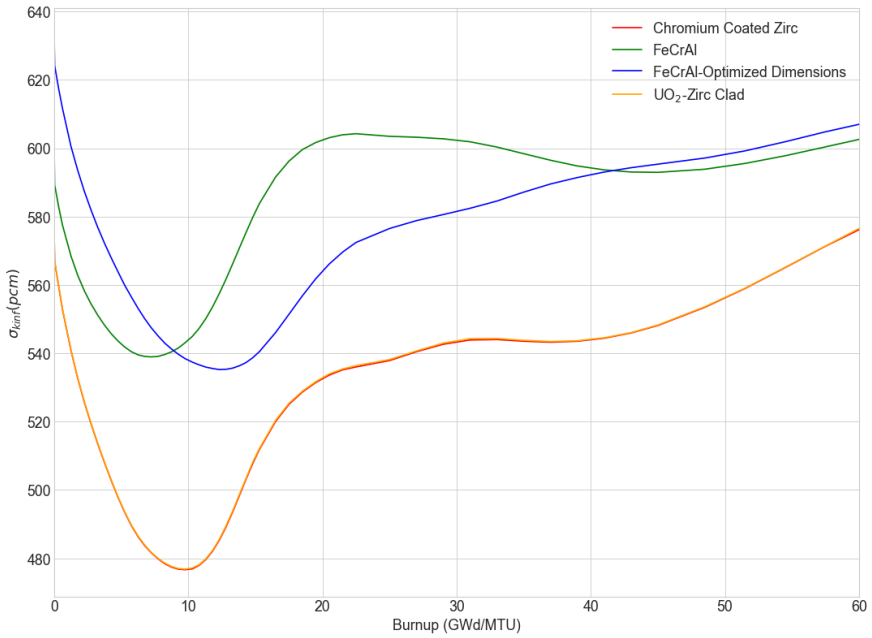

Figure 24. Comparison of standard deviation in BWR lattice k_{inf} with depletion.

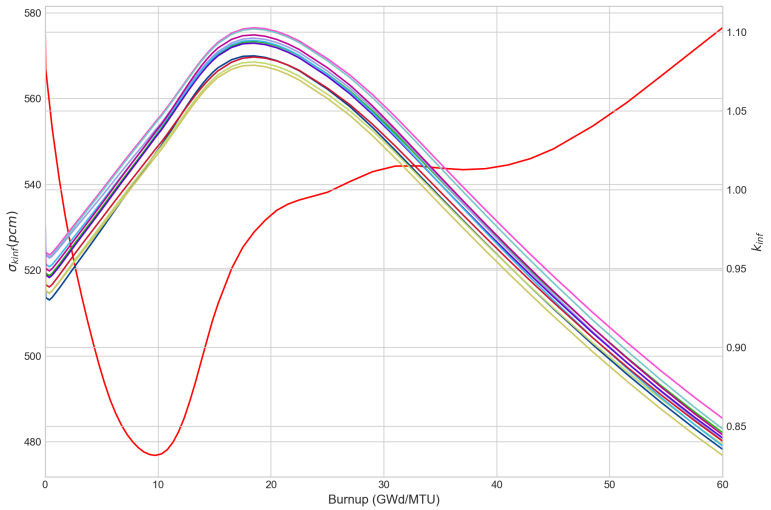

Figure 25. Comparison of k_{inf} with depletion for 10 representative samples generated by SAMPLER for BWR UO_2 lattice

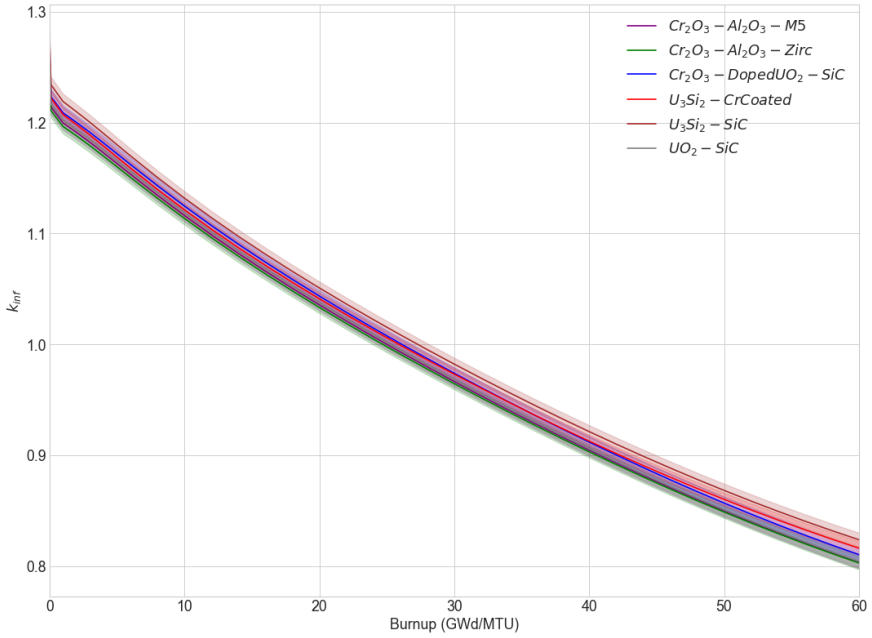

Figure 26. Comparison of PWR lattice k_{inf} with depletion at HFP conditions and cycle-averaged boron.

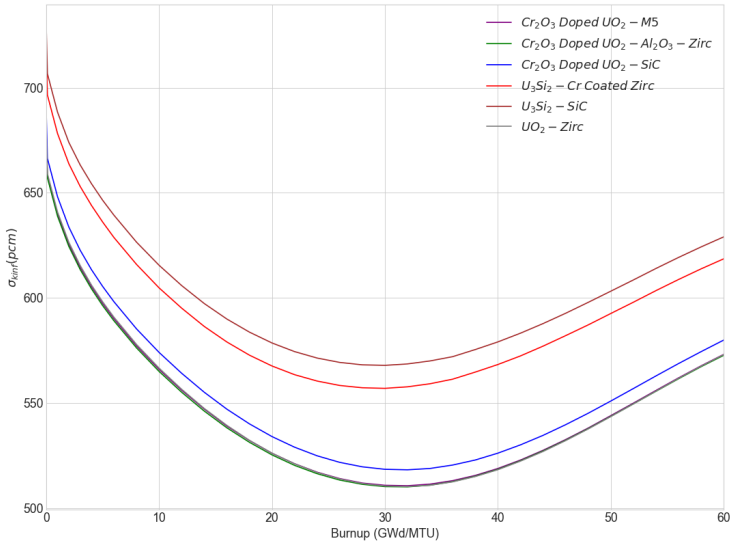

Figure 27. Comparison of standard deviation in PWR lattice k_{inf} with depletion at HFP conditions and cycle-averaged boron.

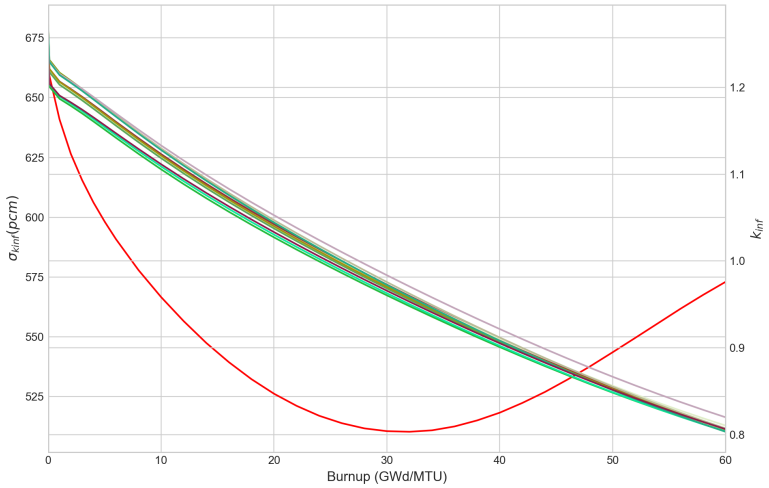

Figure 28. Comparison of k_{inf} with depletion for 10 representative samples generated by SAMPLER for PWR UO_2 lattice.

5. POLARIS CODE ENHANCEMENTS

5.1 NEW INPUT OPTIONS

This section provides an overview of the enhancements to the Polaris code necessary for modeling ATF systems. The first subsection details the additional predefined compositions available, as well as the various ways to include them as fuel dopants. The second subsection demonstrates the new fuel card options available to remove composition definition burdens imposed by fuels other than UO_2.

5.1.1 FUEL DOPANTS

To improve the ease of modeling ATF systems in Polaris, some common ATF dopants were added as predefined compositions. The new predefined compositions include Cr_2O_3, Al_2O_3, and BeO. The three fuel dopants were also added as default system properties of the fuel composition (all with a default value of 0 ppm) for both PWR and BWR models. This flexibility allows for multiple ways to define the same system to achieve an identical system model.

Figure 29 provides three simple pin cell examples of equivalent Polaris inputs for fuel doped with either Cr_2O_3, Al_2O_3, or BeO. The first set of inputs is doped to 1,000 ppm Cr_2O_3, the second set of inputs is doped to 3,000 ppm Al_2O_3, and the last set of inputs is doped to 5,000 ppm BeO. These values do not represent typical fuel doping fractions and are used here only for demonstration purposes. A comparison of the k_{eff} values for these simple pin cell models can be found in Table 20. The marginal discrepancy of no more than 3 pcm for any dopant using the system property definition of the dopant is due to the treatment of composition processing of ^{18}O.

Table 20. Pin cell k_{eff} by dopant

Fuel	Definition	k_{eff}
Cr_2O_3-doped UO_2	Explicit	1.33290
	Predefined	1.33290
	System property	1.33287
Al_2O_3-doped UO_2	Explicit	1.33327
	Predefined	1.33327
	System property	1.33325
BeO-doped UO_2	Explicit	1.33348
	Predefined	1.33348
	System property	1.33345

5.1.2 FUEL COMPOSITION CARDS

Two additional fuel composition cards were added to ease the burden of modeling ATF systems in Polaris. These new cards are specifically intended to be used for modeling systems containing U_3Si_2or UN. The new composition cards are analogous to the UO_2 composition card, but they currently do not support a burnup specification. Both U_3Si_2 and UN composition cards support specifying an enrichment (using the same formulas as the UO_2 composition card) and a reference density.

Figure 30 demonstrates the use of the new U_3Si_2 composition input card. This input models a standard GE 7×7 BWR assembly but has replaced the standard UO_2 fuel with U_3Si_2 enriched to 5.432%. Figure 31 demonstrates the two input variants for the UN composition card. Both inputs are modeling the same 7×7

BWR assembly but have replaced the the UO_2 fuel with the UN fuel. The first example does not specify the ^{15}N enrichment, so the fuel's nitrogen composition is assumed to be 100% ^{15}N. In contrast, the second example explicitly sets the ^{15}N enrichment to match its natural abundance of 0.4%.

A previous deficiency of the ENRU card was also identified and addressed as part of these fuel card enhancements. The documentation of the ENRU card is unchanged from the SCALE 6.2.3 release, so only representative examples of its usage are given here in lieu of a complete input description. Figure 32 provides three simple pin cell input examples demonstrating the use of the ENRU composition card; as with the other examples in this section, these inputs are not realistic and are intended for demonstrative purposes only. The first case defines a metallic uranium fuel enriched to 3.1%. The second and third examples both define a 3.1% enriched UOX pin cell and give identically equivalent results. The second case uses the UOX composition card to define the fuel, while the third case uses the ENRU composition card to define the same exact fuel composition.

5.2 COUPLED LIBRARIES

Two new (n,γ) coupled multigroup (MG) libraries were generated to support coupled (n,γ) calculations in Polaris. The new libraries have both neutron and gamma group structures that correspond to existing SCALE energy structures. The finer resolution library uses the SCALE 252-group neutron energy structure and is coupled to the SCALE 47-group gamma energy structure. The coarser resolution library takes advantage of the SCALE 56-group neutron energy structure and is coupled to the SCALE 19-group gamma energy structure. Both new libraries are neutronically equivalent to their SCALE neutron-only libraries. Since the neutron data on the new libraries are identical to their respective neutron-only SCALE counterparts, the neutron transport calculations will be identical when comparing between the individual coupled libraries and their neutron-only SCALE counterpart.

5.3 GENERATION OF REACTOR LIBRARIES

ORIGEN reactor libraries are used by ORIGEN and ORIGAMI to perform rapid depletion analyses for generation of spent nuclear fuel sources for downstream analysis. In this work, Polaris was updated to generate system-average ORIGEN reactor libraries, similar to the TRITON sequence. This capability will enable analysis of ATF source terms in future work. Before this enhancement, Polaris could only generate an ORIGEN concentrations file stored as "${BASENAME}.f71." Polaris in SCALE 6.3 can generate an ORIGEN library stored as "${BASENAME}.f33". This system-averaged library is automatically generated by Polaris for all depletion calculations.

Three simple models were developed to demonstrate the new Polaris ".f33" file accuracy:

1. Infinite homogeneous case: volume homogenized system of fuel (10.257 g/cc 3.1% enr) and coolant (0.66 g/cc, 1,300 ppm boron), Fuel to volume ratio is 53.6%.
2. Single pin cell case of fuel and coolant. (The infinite homogeneous case is derived from this case.)
3. 2x2 pin cell case where the two enrichments were used (3.1% and 3.6%).

All three cases had the same burnup characteristics:

- 40 W/g constant specific power
- Burnup steps: 0, 0.1, 1, 2, 4, 6, 8, 10, 15, 20, 25, 30, 35, 40
- 1,000-day decay at 40 GWD/MTU

All three cases had the same QOIs:

- Isotope mass at all burnup steps for ^{235}U, ^{236}U, ^{239}Pu, ^{240}Pu, ^{241}Pu, and ^{136}Xe
- Gamma heat after 1000-day decay after 40 GWD/MTU burnup: ^{134}Cs, ^{137m}Ba, ^{106}Rh

For each of the three cases, the Polaris ".f33" file was used to run the equivalent burnup calculation in ORIGAMI. The largest ^{235}U mass difference was 0.6% at 40 GWd/MTU. The largest Pu mass difference at high burnups was 0.7% at 15 GWd/MTU for ^{241}Pu. The largest ^{136}Xe mass difference was 2.3% at 2 GWd/MTU. The relative error in gamma heat QOIs was less than 0.8%.

The errors in time-dependent QOIs are really small, which shows consistent agreement between detailed Polaris depletion and ORIGAMI depletion. In theory, the errors should be 0.0, but errors are unavoidable due to differences in the depletion scheme and substep normalizations.

```
'  Purpose: demonstrate the use of predefined compositions chromia
'  (Cr2O3), alumina (Al2O3), and beryllia (BeO). Here they are added
'  explicitly as a fuel dopant. For each predefined composition, an
'  equivalent input is given that defines the dopant using the FORM
'  card, and another input is given that uses the system property.
'    - Case 1.1-3 run a polaris pincell with UOX fuel doped with Cr2O3
'    - Case 2.1-3 run a polaris pincell with UOX fuel doped with Al2O3
'    - Case 3.1-3 run a polaris pincell with UOX fuel doped with BeO
'    We expect different k-eff for the different dopants, but each
'    triplet should produce identical k-effs regardless of choice of
'    predefined composition, explicit formula card composition, or
'    system property value.
'
' Case 1.1 - UOX fuel doped with Cr2O3 using FORM card
=polaris
title "pincell with UOX fuel doped with Cr2O3 using FORM card"
lib "broad_lwr"
sys PWR
geom wec17 : ASSM 1 1.26
comp uox_e310 : UOX 3.10
comp c_cr2o3 : FORM Cr=2 O=3
comp uox_e310_doped  : WT c_cr2o3=0.1 uox_e310=-100
mat FUEL.1 : uox_e310_doped  10.5
pin 1 : 0.4096 0.418 0.475 : FUEL.1 GAP CLAD
end

' Case 1.2 - UOX fuel doped with Cr2O3 using predefined composition
=polaris
title "UOX fuel doped with Cr2O3 using predefined composition"
lib "broad_lwr"
sys PWR
geom wec17 : ASSM 1 1.26
comp uox_e310 : UOX 3.10
comp uox_e310_doped  : WT CR2O3=0.1 uox_e310=-100
mat FUEL.1 : uox_e310_doped  10.5
pin 1 : 0.4096 0.418 0.475 : FUEL.1 GAP CLAD
end

' Case 1.3 - UOX fuel doped with Cr2O3 using system property
=polaris
title "UOX fuel doped with Cr2O3 using system property"
lib "broad_lwr"
sys PWR
geom wec17 : ASSM 1 1.26
comp uox_e310 : UOX 3.10
mat FUEL.1 : uox_e310  10.5 : cr2o3=1000
pin 1 : 0.4096 0.418 0.475 : FUEL.1 GAP CLAD
end
```

```
' Case 2.1 - UOX fuel doped with Al2O3 using FORM card
=polaris
title "UOX fuel doped with Al2O3 using FORM card"
lib "broad_lwr"
sys PWR
geom wec17 : ASSM 1 1.26
comp uox_e310 : UOX 3.10
comp c_al2o3  : FORM Al=2 O=3
comp uox_e310_doped  : WT c_al2o3=0.3 uox_e310=-100
mat FUEL.1 : uox_e310_doped  10.5
pin 1 : 0.4096 0.418 0.475 : FUEL.1 GAP CLAD
end

' Case 2.2 - UOX fuel doped with Al2O3 using predefined composition
=polaris
title "UOX fuel doped with Al2O3 using predefined composition"
lib "broad_lwr"
sys PWR
geom wec17 : ASSM 1 1.26
comp uox_e310 : UOX 3.10
comp uox_e310_doped  : WT AL2O3=0.3 uox_e310=-100
mat FUEL.1 : uox_e310_doped  10.5
pin 1 : 0.4096 0.418 0.475 : FUEL.1 GAP CLAD
end

' Case 2.3 - UOX fuel doped with Al2O3 using system property
=polaris
title "UOX fuel doped with Al2O3 using system property"
lib "broad_lwr"
sys PWR
geom wec17 : ASSM 1 1.26
comp uox_e310 : UOX 3.10
mat FUEL.1 : uox_e310  10.5 : al2o3=3000
pin 1 : 0.4096 0.418 0.475 : FUEL.1 GAP CLAD
end
```

```
' Case 3.1 - UOX fuel doped with BeO using FORM card
=polaris
title "UOX fuel doped with BeO using FORM card"
lib "broad_lwr"
sys PWR
geom wec17 : ASSM 1 1.26
comp uox_e310 : UOX 3.10
comp c_beryllia : FORM Be=1 O=1
comp uox_e310_doped  : WT c_beryllia=0.5 uox_e310=-100
mat FUEL.1 : uox_e310_doped  10.5
pin 1 : 0.4096 0.418 0.475 : FUEL.1 GAP CLAD
end


' Case 3.2 - UOX fuel doped with BeO using predefined composition
=polaris
title "UOX fuel doped with BeO using predefined composition"
lib "broad_lwr"
sys PWR
geom wec17 : ASSM 1 1.26
comp uox_e310 : UOX 3.10
comp uox_e310_doped  : WT BeO=0.5 uox_e310=-100
mat FUEL.1 : uox_e310_doped  10.5
pin 1 : 0.4096 0.418 0.475 : FUEL.1 GAP CLAD
end

' Case 3.3 - UOX fuel doped with BeO using system property
=polaris
title "UOX fuel doped with BeO using system property"
lib "broad_lwr"
sys PWR
geom wec17 : ASSM 1 1.26
comp uox_e310 : UOX 3.10
mat FUEL.1 : uox_e310  10.5 : beo=5000
pin 1 : 0.4096 0.418 0.475 : FUEL.1 GAP CLAD
end
```

Figure 29. Equivalent dopant definition examples

```
=polaris
%%%%%%%%%%%%%%%%%%%%%%%%%%%%%%%%%%%%%%%%%%%%%%%%%%%%%%%%%%%%%%%%%%%%%%%%%%%%
% setup
%%%%%%%%%%%%%%%%%%%%%%%%%%%%%%%%%%%%%%%%%%%%%%%%%%%%%%%%%%%%%%%%%%%%%%%%%%%%
title "USI fuel in 7x7 GE assembly"
lib "broad_lwr"
sys BWR
%%%%%%%%%%%%%%%%%%%%%%%%%%%%%%%%%%%%%%%%%%%%%%%%%%%%%%%%%%%%%%%%%%%%%%%%%%%%
% materials
%%%%%%%%%%%%%%%%%%%%%%%%%%%%%%%%%%%%%%%%%%%%%%%%%%%%%%%%%%%%%%%%%%%%%%%%%%%%
comp c_usi : USI 5.432
mat FUEL.1  : c_usi 10.2
%%%%%%%%%%%%%%%%%%%%%%%%%%%%%%%%%%%%%%%%%%%%%%%%%%%%%%%%%%%%%%%%%%%%%%%%%%%%
% geometry
%%%%%%%%%%%%%%%%%%%%%%%%%%%%%%%%%%%%%%%%%%%%%%%%%%%%%%%%%%%%%%%%%%%%%%%%%%%%
geom myBWR : ASSM 7 1.875
hgap 0.9
box  0.2 0.9 6.52 : 0.1 : 4.0 : 4.1
pin F : 0.621 0.715 : FUEL.1 CLAD.1
%%%%%%%%%%%%%%%%%%%%%%%%%%%%%%%%%%%%%%%%%%%%%%%%%%%%%%%%%%%%%%%%%%%%%%%%%%%%
% state
%%%%%%%%%%%%%%%%%%%%%%%%%%%%%%%%%%%%%%%%%%%%%%%%%%%%%%%%%%%%%%%%%%%%%%%%%%%%
state ALL  : temp=600
      FUEL : temp=900
      MOD  : void=0
      COOL : void=40
end
```

Figure 30. USI card input example with fuel enriched to 5.432%.

```
=polaris
title "UN fuel with default 100% N-15 enrichment in GE 7x7 assembly"
lib "broad_lwr"
sys BWR
%%%%%%%%%%%%%%%%%%%%%%%%%%%%%%%%%%%%%%%%%%%%%%%%%%%%%%%%%%%%%%%%%%%%%%%%%%%%
% materials
%%%%%%%%%%%%%%%%%%%%%%%%%%%%%%%%%%%%%%%%%%%%%%%%%%%%%%%%%%%%%%%%%%%%%%%%%%%%
comp c_un : UN 4.321
mat FUEL.1  : c_un 10.2
%%%%%%%%%%%%%%%%%%%%%%%%%%%%%%%%%%%%%%%%%%%%%%%%%%%%%%%%%%%%%%%%%%%%%%%%%%%%
% geometry
%%%%%%%%%%%%%%%%%%%%%%%%%%%%%%%%%%%%%%%%%%%%%%%%%%%%%%%%%%%%%%%%%%%%%%%%%%%%
geom myBWR : ASSM 7 1.875
hgap 0.9
box  0.2 0.9 6.52 : 0.1 : 4.0 : 4.1
pin F : 0.621 0.715 : FUEL.1 CLAD.1
%%%%%%%%%%%%%%%%%%%%%%%%%%%%%%%%%%%%%%%%%%%%%%%%%%%%%%%%%%%%%%%%%%%%%%%%%%%%
% state
%%%%%%%%%%%%%%%%%%%%%%%%%%%%%%%%%%%%%%%%%%%%%%%%%%%%%%%%%%%%%%%%%%%%%%%%%%%%
state ALL  : temp=600
      FUEL : temp=900
      MOD  : void=0
      COOL : void=40
end

=polaris
title "UN with N-15 enrichment of natural nitrogen in GE 7x7 assembly"
lib "broad_lwr"
sys BWR
%%%%%%%%%%%%%%%%%%%%%%%%%%%%%%%%%%%%%%%%%%%%%%%%%%%%%%%%%%%%%%%%%%%%%%%%%%%%
% materials
%%%%%%%%%%%%%%%%%%%%%%%%%%%%%%%%%%%%%%%%%%%%%%%%%%%%%%%%%%%%%%%%%%%%%%%%%%%%
comp c_un : UN 4.321 n15enr=0.4
mat FUEL.1  : c_un 10.2
%%%%%%%%%%%%%%%%%%%%%%%%%%%%%%%%%%%%%%%%%%%%%%%%%%%%%%%%%%%%%%%%%%%%%%%%%%%%
% geometry
%%%%%%%%%%%%%%%%%%%%%%%%%%%%%%%%%%%%%%%%%%%%%%%%%%%%%%%%%%%%%%%%%%%%%%%%%%%%
geom myBWR : ASSM 7 1.875
hgap 0.9
box  0.2 0.9 6.52 : 0.1 : 4.0 : 4.1
pin F : 0.621 0.715 : FUEL.1 CLAD.1
%%%%%%%%%%%%%%%%%%%%%%%%%%%%%%%%%%%%%%%%%%%%%%%%%%%%%%%%%%%%%%%%%%%%%%%%%%%%
% state
%%%%%%%%%%%%%%%%%%%%%%%%%%%%%%%%%%%%%%%%%%%%%%%%%%%%%%%%%%%%%%%%%%%%%%%%%%%%
state ALL  : temp=600
      FUEL : temp=900
      MOD  : void=0
      COOL : void=40
end
```

Figure 31. UN card input with and without explicit ^{15}N enrichment specification.

```
' Case 1 - metallic fuel
=polaris
title "pincell with metallic fuel"
lib "broad_lwr"
sys PWR
geom wec17 : ASSM 1 1.26
comp c_enru : ENRU 3.1
mat FUEL.1 : c_enru  19.1
pin 1 : 0.4096 0.418 0.475 : FUEL.1 GAP CLAD
end

' Case 2 - UOX fuel
=polaris
title "pincell with oxide fuel defined by UOX"
lib "broad_lwr"
sys PWR
geom wec17 : ASSM 1 1.26
comp uox_e310 : UOX 3.1
mat FUEL.1 : uox_e310  10.5
pin 1 : 0.4096 0.418 0.475 : FUEL.1 GAP CLAD
end

' Case 3 - UOX fuel defined by formula with ENRU
=polaris
title "pincell with oxide fuel defined by ENRU"
lib "broad_lwr"
sys PWR
geom wec17 : ASSM 1 1.26
comp c_enru : ENRU 3.1
comp uox_e310 : FORM c_enru=1 O=2
mat FUEL.1 : uox_e310  10.5
pin 1 : 0.4096 0.418 0.475 : FUEL.1 GAP CLAD
end
```

Figure 32. ENRU card input variations

6. CONCLUSIONS

This report highlights ATF code assessment activities performed under Project NRC-HQ-60-17-T-0017, Lattice Physics Enhancements and Assessment. ATF covers a broad range of advanced fuel and clad designs for LWRs to enhance performance under several accident conditions. The purpose of this work is to perform initial assessments of the predictive capabilities of NRC neutronics codes that underpin various licensing calculations.

The assessments focus on the SCALE/Polaris lattice physics code. The selected ATF concepts for this report include Cr_2O_3 and Al_2O_3-Cr_2O_3 doped UO_2 fuel, U_3Si_2 fuel, FeCrAl cladding, SiC cladding, and Cr-coated cladding.

The systematic approach taken in this report includes S/U analysis of nuclear data, identification of experimental benchmark and gaps for code validation, investigation of modeling approximations, and code-to-code comparisons of calculated QOIs against high-fidelity reference CE MC calculations.

In terms of the analysis of nuclear data uncertainties and the experiment gap analysis, several key items were identified. It is a significant conclusion that the neither the doping elements, U_3Si_2fuel, or any of the cladding concepts alter these top three contributors to uncertainty: (^{235}U, ^{238}U, and ^{1}H). The addition of FeCrAl cladding introduces ^{56}Fe as a large contributor responsible for the increase in total uncertainty. The validation of BWR lattices is more difficult with the existing suite of critical experiments, and the introduction of FeCrAl cladding exacerbates these difficulties.

In terms of the fundamental physics, the U_3Si_2 fuel form leads to a harder flux spectrum due to a smaller moderator-to-fuel ratio. For the experiment gap analysis, this leads to a larger uncertainty contribution from ^{238}U and a reduction in the number of available experiments available for validation. Additionally, the harder spectrum of the U_3Si_2 fuel models is noticeable in the code-to-code assessment analysis, exhibiting higher ϕ_1/ϕ_2, higher ϵ, and lower p.

In terms of the modeling approximations, one key conclusion is that the reactivity penalty from Cr-coated cladding and FeCrAl cladding is approximately constant as a function of burnup. These cladding forms do not have to be depleted in lattice physics analysis, which is similar to standard cladding. Parametric studies reveal that chromium clad coats can be volume homogenized into the outer 50% of the clad rim without degradation in accuracy while maintaining standard MOC ray spacing parameters.

Model investigations and code assessments reveal a degradation in Polaris modeling accuracy for U_3Si_2 fuel. This is because the library generation procedure to generate self-shielding factors was performed for UO_2-Zry systems. Adjustments will be implemented in this procedure in future work to support higher density fuels such as U_3Si_2 and UN.

Several code enhancements were implemented into SCALE to support ATF. Easy-to-use composition and material properties were added to Polaris to facilitate the process to specify dopant compositions and quantities. Nitride and silicide fuels are now supported in the input file. Polaris can now be used to generate ORIGEN reactor libraries for spent fuel and severe accident analysis for ATF fuel.

REFERENCES

Author unspecified. 2006. *Safety Analysis Report.* Technical report MU Project #000763. University of Missouri, Columbia.

Fensin, M.L. 2004. "Optimum Boiling Water Reactor Fuel Design Strategies to Enhance Reactor Shutdown by the Standby Liquid Control System." Master's thesis, University of Florida.

Jessee, M.A. 2008. "Cross-Section Adjustment Techniques for BWR Adaptive Simulation." Master's thesis, University of North Carolina.

Jessee, M.A., W.A. Wieselquist, T.M. Evans, S.P. Hamilton, J.J. Jarrell, K.S. Kim, J.P. Lefebvre, U. Mertyurek, A.B. Thompson, and M.L. Williams. 2014. "Polaris: A New Two-Dimensional Lattice Physics Analysis Capability for the SCALE Code System." In *PHYSOR 2014—The Role of Reactor Physics towards a Sustainable Future.* ANS PHYSOR Topical Meeting. LaGrange Park, IL: American Nuclear Society.

Marshall, W.J., et al. 2015. *Technical Basis for Peak Reactivity Burnup Credit for BWR Spent Nuclear Fuel in Storage and Transportation Systems.* Technical report NUREG/CR-7194 (ORNL/TM-2014/240). US Nuclear Regulatory Commission.

Marshall, W.J., J.B. Clarity, J. Yang, U. Mertyurek, M.A. Jessee, and B. T. Rearden. 2019. "Initial Application of TSUNAMI for Validation of Advanced Fuel Systems." In *Proceedings of the 11th International Conference on Nuclear Criticality Safety (ICNC2019).* ICNC Topical Meeting. Paris, France: American Nuclear Society.

Marshall, W.J., J. Yang, U. Mertyurek, and M.A. Jessee. 2019. "Preliminary TSUNAMI Assessment of the Impact of Accident Tolerant Fuel Concepts on Reactor Physics Validation." In *Transactions of American Nuclear Society,* 120:500–503. ANS Annual Meeting. LaGrange Park, IL: American Nuclear Society.

Mertyurek, U., et al. 2017. *SCALE Lattice Physics Performance Assessment.* Technical report NUREG/CR-xxxx (ORNL/TM-2017/278). US Nuclear Regulatory Commission.

Rearden, B.T., and M. A. Jessee, Eds. 2016. *SCALE Code System, Version 6.2.3.* Technical report ORNL/TM-2005/39. Oak Ridge, TN: Oak Ridge National Laboratory.

Scaglione, J. M., et al. 2012. *An Approach for Validating Actinide and Fission Product Burnup Credit Criticality Safety Analyses - Criticality (keff) Predictions.* Technical report NUREG/CR-7109 (ORNL/TM-2011/514). US Nuclear Regulatory Commission.

Shapiroa, Rachel A., and Massimiliano Fratonib. 2016. "Assembly Design of Pressurized Water Reactors with Fully Ceramic Microencapsulated Fuel." *Nuclear Technology* 194:15–27.

APPENDIX A. PWR ATF CALCULATION NOTEBOOK

APPENDIX A. PWR ATF CALCULATION NOTEBOOK

The PWR ATF calculation includes three folders: Polaris_Base, Polaris_Restart, and SHIFT_Restart. Each of the three folders contains an input and an output subfolder. The 6 Polaris_Base inputs (5 ATF designs and 1 typical PWR design) are organized as keywords connected by underscores. The first keyword indicates the fuel type, followed by the type of the clad, and finally followed by .inp. An example of the input *U3SI2__COATED_ZR.inp* represents U_3Si_2 fuel with coated Zircaloy clad.

The Polaris_Restart and SHIFT_Restart inputs were generated at 10 burnups using the Polaris_Base output data, resulting a total of 60 Polaris_Restart inputs and a total of 720 SHIFT_Restart inputs. The naming convention for Polaris_Restart inputs is the Polaris_Base inputs followed by a specific burnup in MWd/MTU. For example, the Polaris_Restart input *U3SI2__COATED_ZR_30000.inp* represents U_3Si_2 fuel with ZIRC clad at 30 GWd/MTU. The naming convention for SHIFT_Restart inputs is the Polaris_Restart inputs followed by a branch number. For example, the SHIFT_Restart input *U3SI2__COATED_ZR_30000_05.inp* represents U_3Si_2 fuel with ZIRC clad at 30 GWd/MTU for branch 5. The layout for the directory structure is provided in Figure 33.

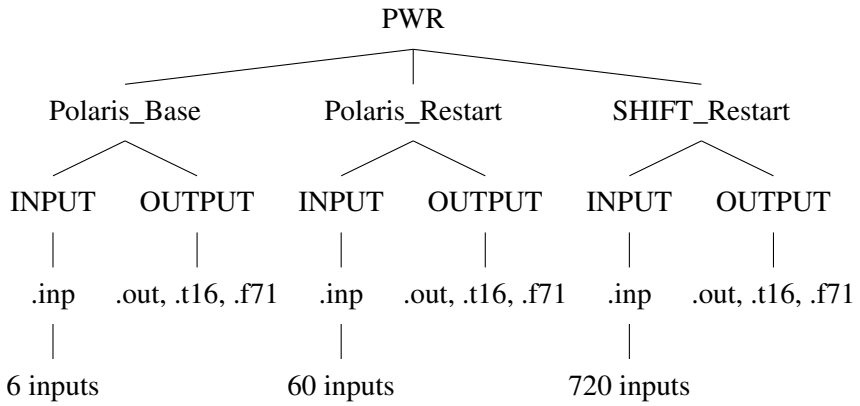

Figure 33. PWR input and output layout.

APPENDIX B. BWR ATF CALCULATION NOTEBOOK

APPENDIX B. BWR ATF CALCULATION NOTEBOOK

The BWR ATF calculation contains two folders: Polaris and CE-KENO. Each of the two folders contains an input and an output subfolder, with a total of 6 inputs. The naming convention of the inputs is very similar to that of the PWR ATF input. The inputs are organized as keyword triplets connected by underscores. The first keyword indicates the BWR type, followed by the fuel type, followed by the type of clad, and finally followed by .inp. The input *GE14DOM_UO2__COATED_ZIRC2.inp* represents GE design UO_2 fuel with Zircaloy-2 clad. The layout for the directory structure is provided in Figure 34.

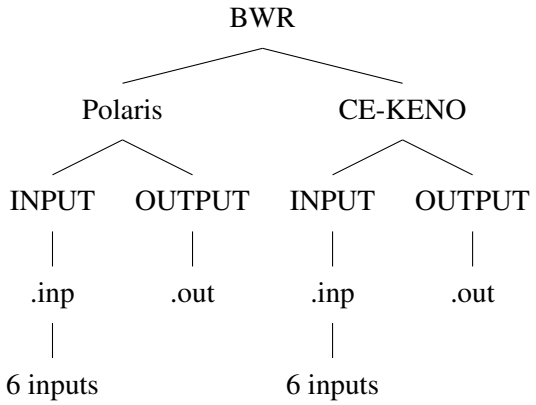

Figure 34. BWR input and output layout.